Schweizerische Eidgenossenschaft
Confédération suisse
Confederazione Svizzera
Confederaziun svizra

Département fédéral de l'environnement,
des transports, de l'énergie et de la communication DETEC

Office fédéral de l'énergie OFEN
Section Cleantech

Rapport final du 30 avril 2019

DCSMART

DC distribution in smart grids

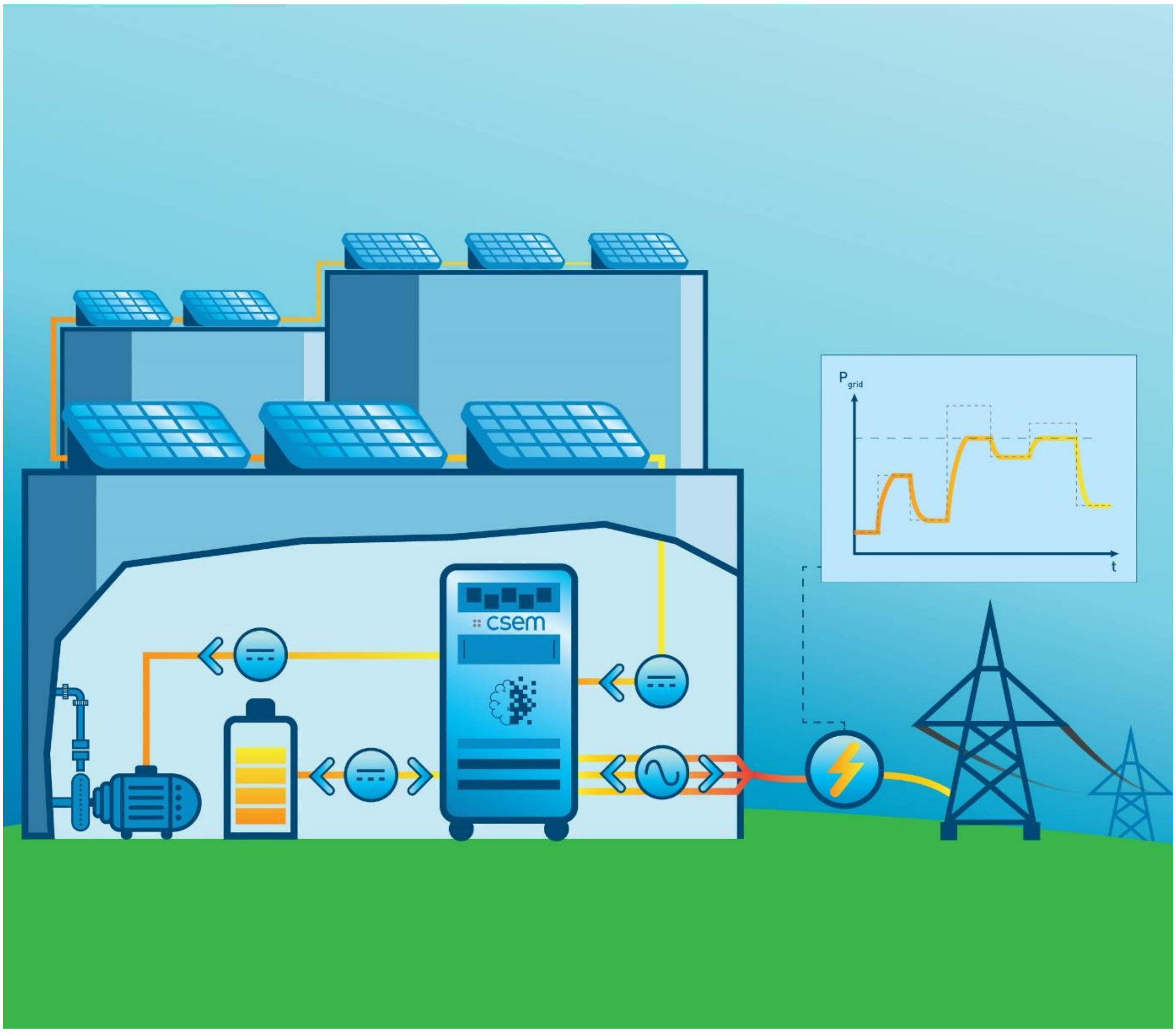

Date : 30 avril 2019

Lieu : Neuchâtel

Prestataire de subventions :
Confédération suisse, représentée par
L'Office fédéral de l'énergie OFEN
Programme pilote, de démonstration et Programme-phare
CH-3003 Berne
www.ofen.admin.ch

Bénéficiaires de la subvention :
CSEM
Jaquet-Droz 1, Case postale, CH-2002 Neuchâtel
www.csem.ch

Viteos SA
Quai Max-Petitpierre 4, Case postale 3206, CH-2001 Neuchâtel
www.viteos.ch

Auteurs :
Pierre-Jean Alet, CSEM, pierre-jean.alet@csem.ch
Nelson Koch, CSEM, nelson.koch@csem.ch

Direction du programme de l'OFEN :	Yasmine Calisesi, yasmine.calisesi@bfe.admin.ch
Suivi du projet pour l'OFEN :	Michael Moser, michael.moser@bfe.admin.ch
Numéro du contrat de l'OFEN :	SI/501375-01

Les auteurs sont seuls responsables du contenu et des conclusions de ce rapport.

Office fédéral de l'énergie OFEN
Mühlestrasse 4, 3063 Ittigen, Adresse postale : 3003 Berne
Tél. +41 58 462 56 11 · fax +41 58 463 25 00 · contact@bfe.admin.ch · www.ofen.admin.ch

Zusammenfassung

Das Projekt ERA-Net DCSMART verfolgt das Ziel, Gleichstromtechnologien für den Einsatz in Smart Grids zu entwickeln. Das hier beschriebene Pilotprojekt, das den schweizerischen Beitrag zu diesem europäischen Projekt darstellt, konzentriert sich auf die Integration von Photovoltaik und nativen Gleichstromverbrauchern in Verteilnetze. Das Pilotprojekt zielt speziell auf einen industriellen Kontext mit der Kombination von PV-Produktion, Batteriespeicher und Industriemotoren ab. Der Schwerpunkt der Untersuchung liegt auf der Erbringung von Dienstleistungen, die solche Mikronetze erbringen können, sowie deren Auswirkungen auf die Servicequalität im Verteilernetz.

Résumé

Le projet ERA-Net DCSMART vise à développer des technologies de distribution à courant continu pour faciliter le déploiement de réseaux intelligents. Le projet pilote décrit ici, qui représente la contribution suisse à ce projet européen, se concentre sur l'intégration de l'énergie photovoltaïque et des consommateurs natifs de courant continu dans les réseaux de distribution. Le projet pilote vise spécifiquement un contexte industriel avec la combinaison de la production photovoltaïque, du stockage de batteries et des moteurs industriels. L'enquête porte principalement sur la prestation des services que ces micro-réseaux peuvent fournir ainsi que sur leur impact sur la qualité du service sur le réseau de distribution.

Abstract

The ERA-Net DCSMART project aims to develop DC distribution technologies to facilitate the deployment of smart grids. The here described pilot project, which represents the Swiss contribution to this European project, has a focus on the integration of photovoltaics and native DC consumers into distribution networks. The pilot specifically targets an industrial context with the combination of PV production, battery storage and industrial motors. The focus of the investigation is on the provision of services that such microgrids can provide as well as their impact on the quality of service on the distribution network.

Take-home messages

- A microgrid with direct current distribution is operational in an industrial environment and integrates PV production, battery storage and industrial motors
- The delivery of multiple services (control of power ramps, peak power shaving, self-consumption) makes a battery storage system always more financially attractive than if it is only dedicated to self-consumption
- The CSEM has developed and patented a control strategy to provide these services. It is applicable to direct current and alternating current.
- An economically attractive case for the control strategy developed may be the self-consumption communities

Table of contents

Starting context

The ERA-Net DCSMART project aims to develop DC distribution technologies to facilitate the deployment of smart grids. The pilot project represents the Swiss contribution to this European project.

The main application of the technologies implemented in this pilot is the integration of photovoltaics into the distribution networks. They are particularly applicable to medium power installations (from 10 kW to 1000 kW) on industrial or commercial buildings. This segment represents about one third of the global photovoltaic power market.[1] This corresponds to about 130,000 new installations in 2014 worldwide, and more than 200,000 in 2020. In Switzerland, this segment represents 90% of the market, or about 3,000 new installations in 2014.[2]

There is an industrial base for the supply of components (storage systems, converters, protection systems) in Switzerland (e. g. Leclanché, Maxwell, ABB, Studer Innotec) and abroad (e. g. Panasonic, SolarEdge, Moixa Technology, Vicor). The integration and control of DC microgrids, on the other hand, was a poorly developed activity at the beginning of the project, focused on niche applications such as the power supply of islands[3] and that of data centers.[4], [5]

Direct current distribution is already used commercially in some data centers.[4] The electrical architecture is extremely specific; the motivations are energy efficiency, investment costs, and reliability. These systems generally do not include control or generation. However, this application has led to the first standardization efforts in the field.[6], [7]

For more general applications, various pilot projects and demonstrations of DC microgrids exist around the world. The technological references at the beginning of the project were:

- European DCC-G project, in which demonstrators have been set up in Philips Research [8] (Netherlands) and Fraunhofer IISB [9] (Germany, DC SMART partner)
- Low-voltage research grid [10] of the Lappeenranta University of Technology (LUT, Finland), in which the distribution is carried out in direct current on certain branches but where the buildings, interfaced by inverters, operate in a conventional way by alternating current
- "Living laboratories" at the University of Aalborg (Denmark) and the Electrical Engineering University of North China [11, p.], still in the design phase, reproducing residential buildings in a controlled manner
- Residential demonstration buildings ("DC Eco House") including photovoltaic generation and DC loads, implemented by Sharp in Japan [12] and the United States
- Microgrids installed by Bosch in commercial buildings (warehouses) equipped with photovoltaic generation and LED lighting.[13]

Apart from the demonstrator from the Lappeenranta University of Technology, all these pre-existing projects focused on the internal performance of buildings, in particular on the local and efficient consumption of photovoltaic electricity. Thus, Bosch's study showed an energy gain of 6% to 8% compared to comparable AC microgrids. Philips' showed gains of 2% for a power of 2 kW, and the potential for gains of 5% for a power of 8 kW or more. None of the pre-existing projects addressed the interaction between DC microgrids and the broader power system; in particular, the services that these microgrids can provide to the system and their impact on quality of service had been ignored in the demonstration projects.

The project is part of a European collaboration within the framework of the ERA-Net Smart Grids Plus. Only one Swiss partner, the CSEM, is involved in this collaboration. The other European members of the consortium are based in the Netherlands and Germany:

1. Delft University of Technology (TU Delft): TU Delft coordinates the European collaboration. The scientific coordinator is Dr Pavol Bauer, director of the group "DC Systems, Energy Conversion and Storage" and the administrative manager is Mr Ernst Harting, from the recovery centre. Four groups of the TU Delft are involved in the collaboration:
    a. DC systems, energy conversion and storage: the group designs and analyses DC systems for the conversion, distribution and use of electricity, in particular to integrate renewable energy sources and electric vehicles. Its skills are in power electronics and electrical engineering. It has 500 m² of laboratories. This group is in charge of the technical coordination of the project, the development of DC electronic transformers, the development of algorithms to ensure stability and manage congestion in a DC distribution network, and modelling and evaluation tasks for the Dutch demonstrator
    b. Architecture: the group specializes in the integration of sustainable development into urban planning. He is in charge of the integration of the low voltage direct current network in residential buildings, in particular the impact on spatial organization
    c. Algorithmic: the group develops algorithms for decision-making in uncertain contexts, with an emphasis on applications to smart energy grids. He is in charge of the development of electricity market models
    d. Energy and industry: the group studies the adequacy of electricity generation and the structure of electricity markets. It will contribute to the development of electricity market models
2. Eindhoven University of Technology (TU Eindhoven): the "Electromechanical and Power Electronics" group models, analyses, designs and optimizes energy conversion systems. The main research focus is on converters with multiple ports and advanced functions. It is in charge of the development of a bidirectional DC/DC converter with isolated transformer.
3. Fraunhofer Institute for Integrated Systems and Component Technologies (Fraunhofer IISB): The "DC Networks" group, within the "Power Electronics" division, develops DC/DC converters as well as architectures and control systems for DC microgrids. It is in charge of developing a converter for local phase management for connection to the "two-phase" distribution network, designing communication interfaces, and specifying and developing electronic current limiting components for operational safety.
4. Direct Current BV (DCBV) is a consulting and engineering company specialized in direct current infrastructure. It is in charge of the Dutch demonstrator and the exploitation of the results.

Basis, framework conditions

The growing interest in DC microgrids comes from the observation that electrochemical storage, photovoltaic generation, and an increasing number of electrical loads (LED lighting, computers, variable speed motors) operate natively on DC or have a DC stage. Benefits include a reduction in the size and increased efficiency of converters[14], [15], conceptual simplification, reduction of overall system losses by up to 15% in the case of high demand and in the presence of storage. It is also easier to decouple microgrid control from network conditions than in the case of alternating current, which reinforces the concept of microgrid, thanks to interface converters.

The proposed control strategy for the DC microgrid is based on the "DC bus signalling" technique: the various system components react autonomously to the change in voltage on the main DC bus compared to its nominal value. It differs from existing approaches by introducing different dynamics for the bidirectional inverter and for the converter feeding the storage. The sizing and programming of these two converters is therefore the central point of the proposed approach.

Concept - description of the installation

The pilot was planned in a public industrial site, the water treatment plant of the City of Neuchâtel (WTP). This site already included a biogas production facility used for local electricity production. The grid operator and energy supplier of the cities of Neuchâtel, La Chaux-de-Fonds and Le Locle, Viteos, is working on a project to store electricity by chemical means ("power to gas") in connection with photovoltaic generation. A photovoltaic solar power plant was therefore planned on site. The two projects had a good thematic complementarity around the integration of distributed and intermittent energies into the electricity system: on the one hand, seasonal management with long-term storage in gaseous form, and on the other hand, local management and use of electricity produced at short time scales with the DC SMART project.

The proposed approach consists of the integration and control of different hardware components. Its commercial application is therefore the responsibility of network managers, photovoltaic installers and, to a lesser extent, conventional electrical integrators. It may also be of interest to component suppliers wishing to expand their offer.

Energy production and consumption at Neuchâtel WTP

The Water Treatment Plant (WTP) of Neuchâtel not only treats the waste water of the city and its neighbourhood (nearly 7 million cubic meters) but is also an important contributor to various local energy networks, mainly the medium voltage electrical grid and the local district heating.

Indeed, regarding the district heating, Neuchâtel WTP recently commissioned a Combined Heat and Power (CHP) unit. This unit valorises the biogas produced by the different biological and chemical processes of the water treatment. The produced heat (2.5 million kWh) and power (2 million kWh) are primarily destined to cover the WTP own needs, with the extra productions fed to the local grid and distributed to nearby consumers. Moreover, on the electrical side, most of the WTP rooftops are now covered with photovoltaic panels exploited by the local utility company, thus reinforcing the City commitment to the promotion of renewable energy sources.

From this point of view, the selection of this public premises to implement the Swiss demonstrator of a DC micro-grid takes all its sense. Indeed, the perspective of integrating innovative technologies to reduce the overall energy consumption and improve the energy efficiency fully integrate in this trend.

Figure 1 presents a complete overview of the energy production and consumption on this site.

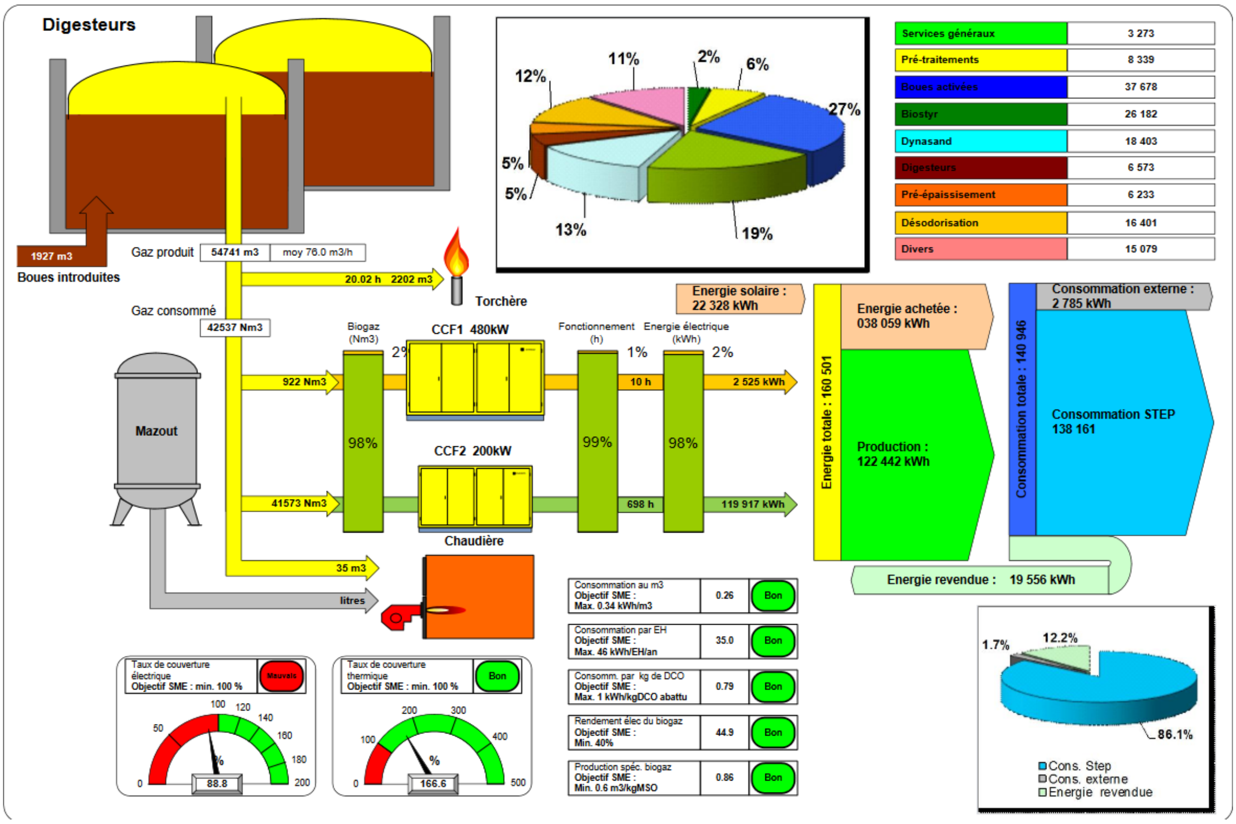

Figure 1: Overview of energy production and consumption on the Swiss demonstration site; source: Service des infrastructures de la Ville de Neuchâtel.

On-site electricity production currently comes from:

- Solar PV (181 MWh/yr)
- Biogaz CHP (1’540 MWh/yr)

On-site electricity consumption is 1’859 MWh/yr. The resulting self-sufficiency and self-consumption ratios are 78% and 84% respectively.

Target building

The initial goal of the Swiss Demonstration Site (SDS) was to improve the energy consumption of the administrative building of Neuchâtel WTP, especially through the installation of LED lighting and electrical heating and/or cooling systems, the intrinsic flexibility of which could be used to implement demand side management strategies.

However, after discussions with Neuchâtel WTP staff, it appeared that the considered building had already been recently equipped with such lighting systems. Moreover, the whole WTP site is connected to the district heating and the local free-cooling system, which eliminates the need for electrical heating or cooling.

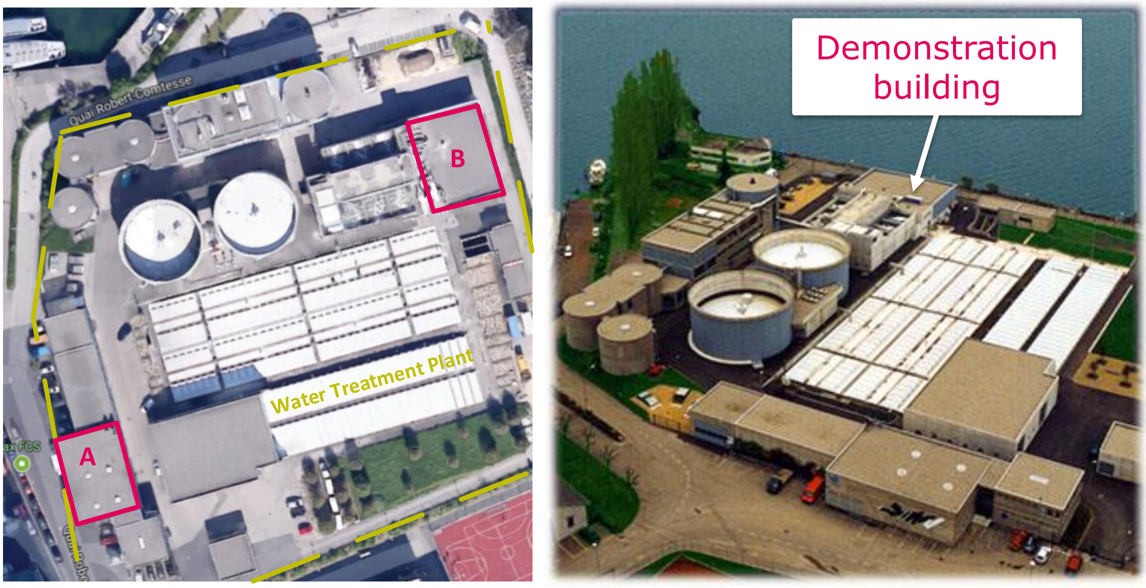

Figure 2: Neuchâtel WTP with the administrative building (A) and the industrial one where the SDS will be installed (B). Source: Service des infrastructures de la Ville de Neuchâtel.

The decision has thus been taken to integrate the Swiss demonstrator into one of the industrial building of Neuchâtel WTP (Figure 2) where many processes, with significant electrical energy consumptions, are present, thus adding significance to the project results. Indeed, industrial installations present a far greater potential for technology transition due to the more important influence such customers can have on the market and the bigger diversity of the encountered applications.

Target loads: industrial motors

Existing motors on the plant

At the project beginning, it was planned to integrate in the demonstrator loads already in use in the industrial part of Neuchâtel WTP. These loads were frequency converters used to drive induction motor destined to applications such as ventilation or pumping.

Figure 3: Frequency converter initially selected for integration in the demonstrator

These frequency converters provide DC terminals, normally intended for plugging braking resistors. It was planned to use these same terminals to connect these frequency inverters to the developed micro-grid.

Nevertheless, test conducted on a spare device have shown that such a connection was not possible. Indeed, the voltage measured between the DC terminals seems to depend on the converter state, as schematized on Figure 4. More precisely, a near zero value has been measured with a stopped motor. This is most probably due to the presence of an internal transistor the purpose of which is to enable or disable the braking resistors.

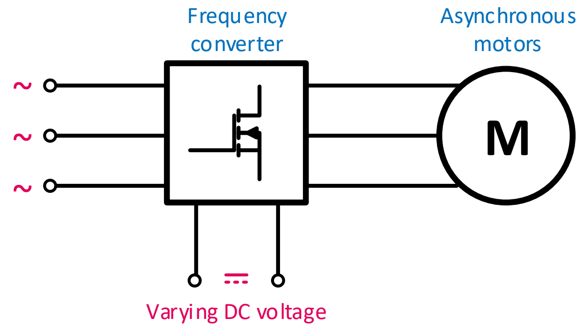

Figure 4: illustration of the varying voltage issue

An alternative solution consisting in supplying the frequency converter through the front-end diode rectifier, as illustrated on Figure 5, has been investigated.

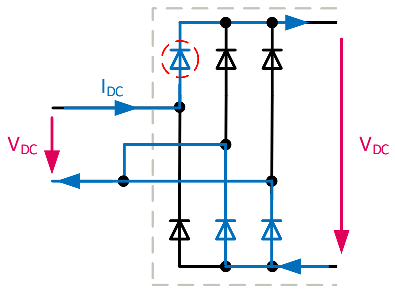

Figure 5: overheating issue caused by a DC supply through the rectifier

Even if this solution allows to solve the varying voltage issue, it introduces another one. Indeed, even if it is possible to connect two legs in parallel in order to split in two either going or returning current, one of the diode will permanently carry the full current. This will introduce overheating issues since the cooling system has been designed in order to accommodate diodes conducting during only one third of the time.

Even if working from a functional point of view, this solution has been rejected due to the probable associated reliability issues that it would have raised and which are unacceptable in the context of a 24/7 exploitation.

Therefore, an alternative solution had to be developed, as described in section at page 15. This solution has been designed to replicate the consumption behaviour of the loads in use at Neuchâtel WTP, allowing to exploit the results almost as if the measurements had been taken on the real system.

Energy consumption

Figure 6 illustrates a typical week of consumption of one the ventilation unit of Neuchâtel WTP. The time origins corresponds to 7 am of the first recorded day.

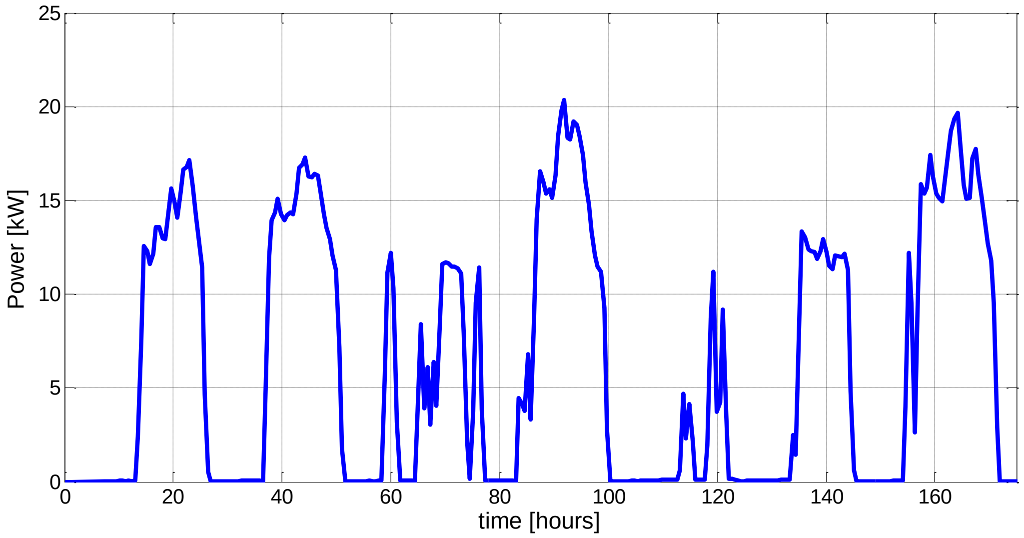

Figure 6: Consumption profile of the ventilation unit of Neuchâtel WTP

This consumption profile clearly shows a daily pattern, characterized by important peaks and a consumption going down to zero. One can also observe that the peaks occur at night and are therefore not aligned with the PV production.

From these observations, it seems that applications with such power profiles could greatly benefit from the increased self-consumption and peak-shaving services that the DCSMART approach could provide.

Photovoltaic production

Based on the remaining available space on WTP rooftops and discussions with the people managing Neuchâtel WTP, a photovoltaic system with a rated power of 10 kWp has been agreed upon. This power rating corresponds to a trade-off between budget constraints and the needs of the developed DC micro-grid and those of Neuchâtel WTP. Indeed, it is currently planned to integrate the photovoltaic installation in the low-voltage AC grid of Neuchâtel WTP at the project completion.

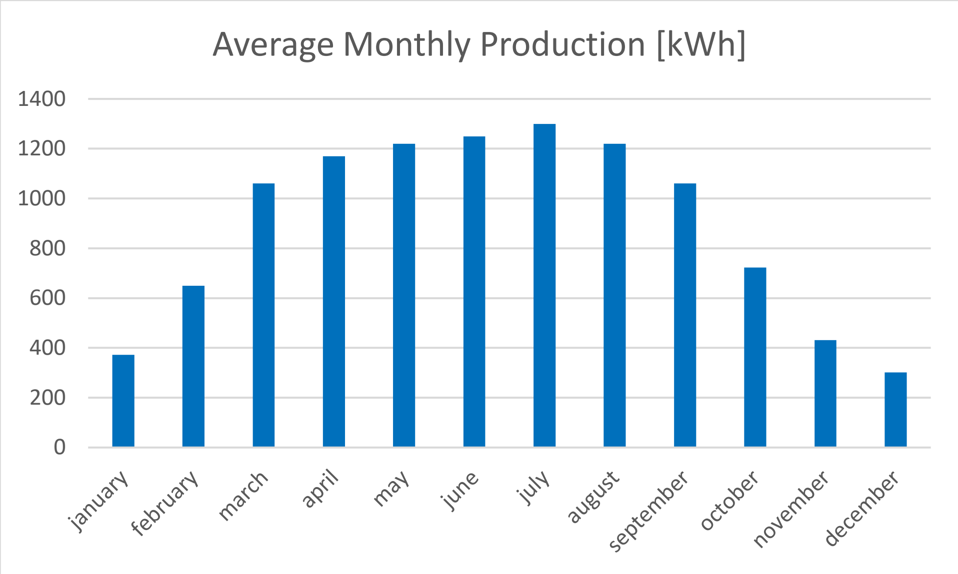

Figure 7: Production estimation for the considered system

Figure 7 shows an estimation, as calculated with PV-GIS,[1] of the monthly production based on parameters presented in Table 1. The system inclination (angle relative to the horizontal plane) and orientation (angle relative to the direction of the South) corresponds to optimal parameters computed by the prevision tools based on the system location. The estimated losses include the losses related to the temperature and the low irradiance, the angular reflectance effects and the electrical losses.

Table 1: Parameters of the considered photovoltaic system

Rated power	Inclination	Orientation
10 kWp	35 °	-1°
Position	**Technology**	**Estimated total losses**
46°59'39" N, 6°56'49" E	Crystalline silicon	23.5 %

A yearly average production of approximately 10’800 kWh is expected.

Structure of the demonstrator

Additional services for DSO and final users

At the beginning of the project it was planned to upscale the previously developed control strategy[16] from a table-top demonstrator to a full size system, where the main goal was to improve the quality of the power exchanged with the AC distribution grid by reducing its variability. This approach is known as ramp-rate control.

[1] http://re.jrc.ec.europa.eu/pvgis/

Even if its contribution to grid stability can be particularly significant in weak grids, such as those that can be found in developing countries, the power variability doesn't have consequences of such importance in the strong and stable European grids.

For this reason, additional services have been included in the control strategy for the implementation in the Swiss demonstration site: the limitation of the exchanged power, known as peak shaving, and the increase of the local consumption of the locally produced energy, also named self-consumption. These services benefit both DSOs and final users.

Indeed, costs of distribution grids are mainly linked to their rated power and only marginally to the transiting energy. For this reason, curtailment is more and more often mentioned as a solution allowing to increase the RES penetration, like in Germany where a limitation to 70% of the rated power of PV installations is mandatory.[17]

For the same reason and due to the emergence of prosumers, DSOs are currently expressing a will to charge the energy distribution based also on the maximum exchanged power and not only on the consumed energy anymore.[18]

Thus, it can be interesting for final users whose energy consumption shows important power peaks to be equipped with a system allowing to reduce this maximum exchanged power while ensuring the correct operation of their different appliances.

Finally, because of decreasing incentives for energy injection in the distribution grid, local consumption of energy produced by distributed RES is more and more interesting for the final user. If this consumption is not aligned with the production, an energy storage system (ESS) with an appropriate control strategy is needed.

General topology

The final system is schematically represented on Figure 8.

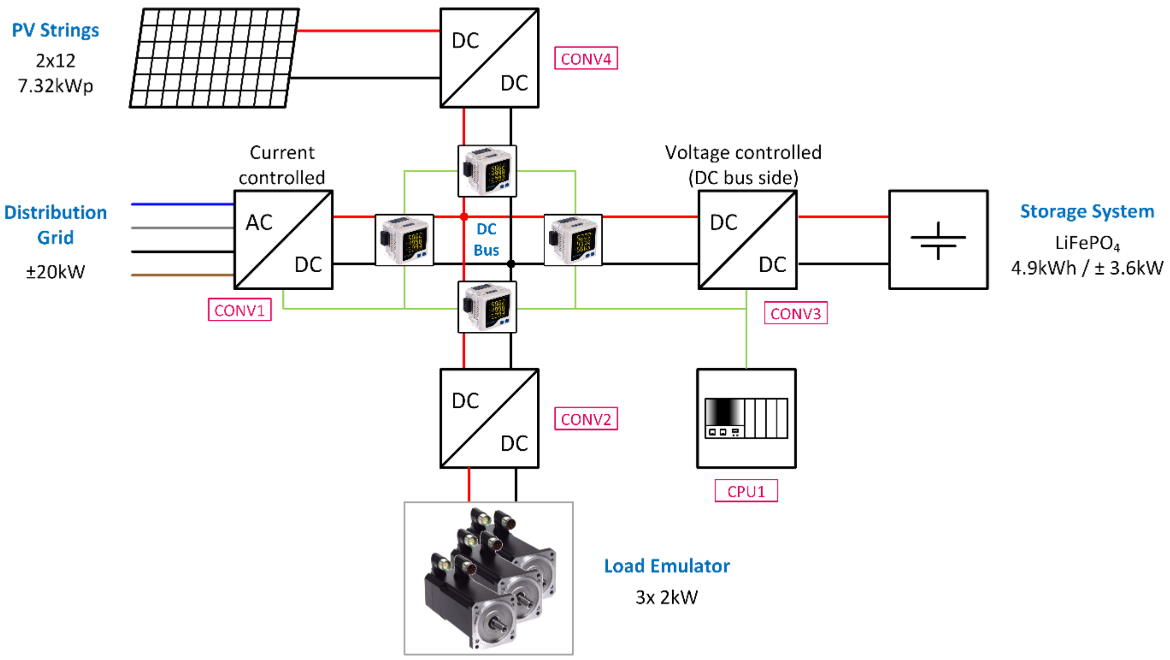

Figure 8: General topology of the Swiss Demonstrator

Main components

This system is composed of the following elements:

- A single bidirectional AC/DC converter (CONV1), which interfaces the DC micro-grid with the up-stream AC low voltage distribution grid. This converter is linked to a local controller in order to compute voltage, current, and power set-points. The DC side of this grid-tied converter is the common DC-link to which all the micro-grid elements are connected.
- A photovoltaic system, represented by a PV module and its DC/DC power optimizer (CONV4).
- A central control unit (CPU1), the roles of which are the system supervision and the transmission of set-points to the different local controllers.
- A DC/DC converter (CONV2), supplying loads with adequate voltages.
- An energy storage system connected to the DC bus through a DC/DC converter (CONV3). Although initially planned to be directly connected to the DC bus, without interface converter, this solution has been abandoned after the selection of the energy storage system. Indeed, in addition to safety reasons, the selected low voltage lithium iron phosphate battery cannot be directly connected to the high voltage DC bus.
- Smart-meters connected to each of the different feeders whose measurements are gathered and stored in the central control unit.

Figure 9: Swiss Demonstrator Main cabinet

Figure 9 illustrates the main cabinet of the SDS, which contains the grid-tied AC/DC converter, the protection system, and local and central control units, the various smart-meters and the stabilizing DC/DC converters. The energy storage system is hosted in a separated rack.

Power flows

Figure 10 graphically defines the different power flows occurring in the system depicted on Figure 8. Blue and red arrows respectively define positive and negative flows for the different elements according to the sign convention used in this document.

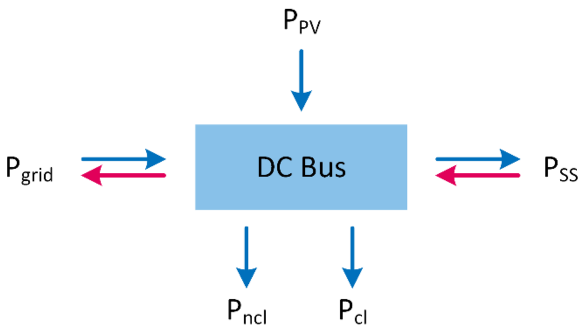

Figure 10: Definition of power flows, where P_{PV} is the photovoltaic power, P_{SS} is the storage system power, P_{ncl} and P_{cl} are respectively the non-controllable and controllable load power and P_{grid} is the grid power.

Thus, the internal power balance P_{bal} is defined according to the following equation:

$$P_{bal} = P_{PV} - P_{ncl} - P_{cl}$$

Therefore, a positive power balance means a local production larger than the local consumption. In such a case, the excess production is either stored in the ESS or rejected to the upstream AC distribution grid.

On the other hand, a negative power balance means that the local consumption exceeds the local production. In such cases, the required additional power is provided either by the distribution grid, through the interface AC/DC converter, or by the Energy Storage System, depending on its state of charge (SoC).

Purpose-built load system

The initially planned loads from WTP have proved to be incompatible with the developed demonstrator. Nevertheless, a system aiming at replicating their energy consumption has been developed. This system is illustrated on Figure 11.

Figure 11: Purpose-built load system of industrial motors

This system is composed of three distinct subsystems made of DC/AC converters, permanent magnet synchronous motors and magnetic powder breakers supplied by a common insulated DC/DC converter, mandatory to stabilize the applied DC voltage and due to the grounding of the return wire of the common DC-link.

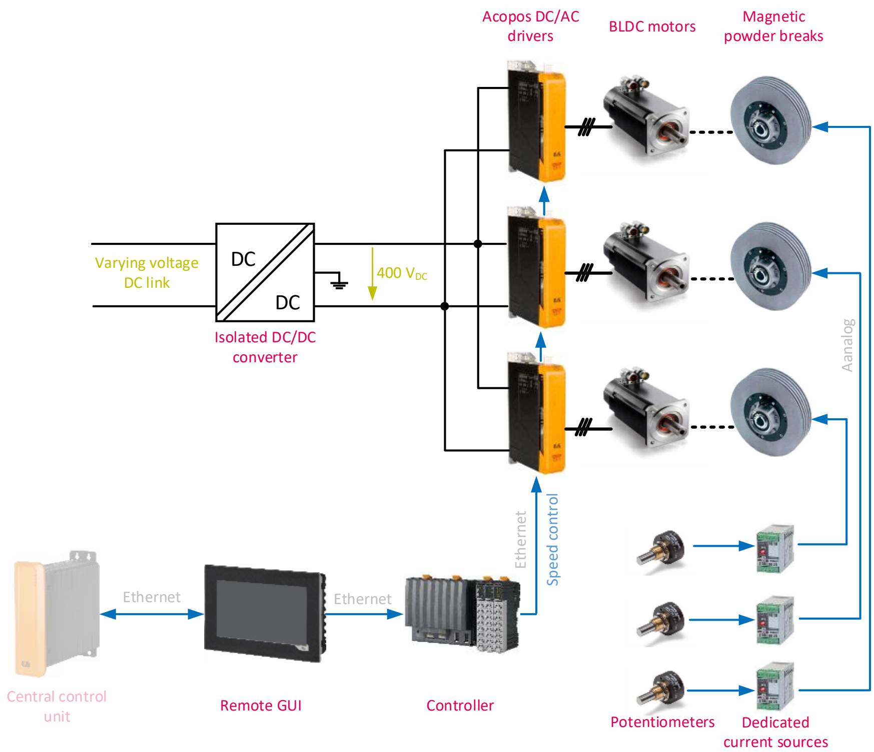

Figure 12: Components of the purpose-built load system

Speed cycles can be defined on a remote graphical interface that can eventually be duplicated on the central control unit. These speed cycles are then processed in a PLC that ensure the speed control of the motors through an internet communication with the DC/AC inverters. Finally, potentiometers linked to dedicated current sources allow to control the resistive torque applied to the magnetic breaks that are cooled by fans that are not represented.

Bill of material

Since finding compatible devices may be an important issue when developing DC distribution systems, a summary of the most important pieces of equipment is given is this section, under the form of Table 2. A short description of each component is given after this table.

Table 2: Bill of main pieces of equipment

#	Device/Function	Manufacturer	Reference
1	Controllable AC/DC converter	Regatron	TopCon TC.GSS
2	DC smart meters	Accuenergy	Acu243
3	DC differential protection relays	Dossena	DER3BDUAL/6D

4	DC circuit breakers	ABB	S802PV
5	Controllable drives with DC inputs	B&R automation	8EI8X8HWS10.0600-1
6	DC/DC string optimizer	AMPT	V750 13.5
7	DC/DC battery converter	MSc Electronics Oy	80DCDC750DE

- Controllable AC/DC converter: This bidirectional AC/DC converter is able to supply a positive DC voltage (up to 600V) with a positive or negative current. It can operate either in constant voltage, constant current or constant power modes. Moreover, it can be controlled by many interfaces, the simplest one being a set of digital and analogue inputs.
- DC smart meter: These meters are equipped with a RS-485 communication interface that allow them to be easily integrated in a larger system. Moreover, they provide a lot of advanced measurements such as the total drawn or injected energy. The used model uses direct voltage sensing and remote hall-sensors for current sensing.
- DC differential protection relays: These differential protection relays use remote current sensing hall sensors to provide a protection against accidental grounding.
- DC circuit breakers: These breakers are standard industrial ones, mainly used in photovoltaic installations.
- Controllable drives with DC inputs: these drives, used in conjunction with B&R automation motors, provide DC terminals alongside the classical AC ones. These terminals are nominally used to parallel different motors in order to feed the breaking energy of the decelerating ones to the other ones, the rectifier stage being a diode bridge. In the case of the Swiss Demonstrator, these terminals are directly connected to a stabilized DC voltage provided by an insulated DC/DC converter fed by the general DC-link.
- DC/DC string optimizers: These optimizers have been selected here for their ability to work with varying voltage on the DC-link stage.
- DC/DC battery converter: Bi-directional and voltage controlled converter. The purpose of this converter is to adapt the voltage levels.

Procedure / methodology

Control strategy: objectives, design and simulation

The control strategy developed by CSEM for the Swiss demonstration site aims at providing three smart grid services:

- Increase in local, self-consumption of locally-produced renewable electricity. This service is mainly of benefit to the end user (prosumer) who can thus reduce their electricity bill. When combined with other services it can also provide benefits to the wider distribution system since it reduces the load on the distribution network.
- Limitation of upward and downward ramp rates. This service is of benefit to the distribution system only. Indeed, it makes it easier for distribution system operators and other grid operators to operate their assets since it makes the grid more predictable. This feature is currently mandated by regulation in some island grids but in continental Europe there is no way to monetize it yet.

– Reduction in peak power. This service is of technical benefit to the distribution network operator, since reducing the peak load translates into reduced investment need. Thanks to the peak-power component of the electricity bill, which is commonly applied to commercial and industrial users, this service is also of economic benefit to the end user.

Figure 13 illustrates the topology of the implemented control strategy that is split in three different levels: the physical system, the first control level characterized by fast and simple controllers, and the supervision level where more advanced and slower control technics are used. More details about these levels are given below.

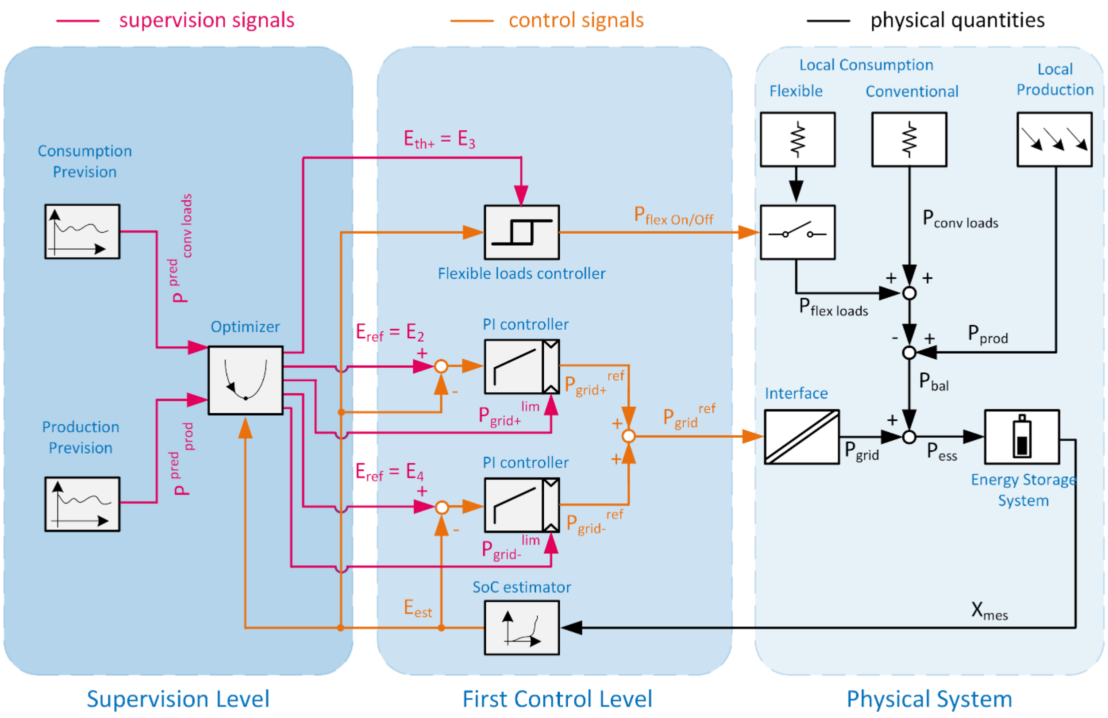

Figure 13: Layers and detailed implementation of the control strategy

On the lowermost level, the physical system, and as previously mentioned, the active and controllable elements are the AC/DC interface converter and the DC/DC converter supplying the flexible loads, here represented as a switch. The first one acts on the system by extracting power from or injecting power to the grid while the second can turn on or off the controllable loads.

These devices act on information coming from the first control level. There, the state of the complete system i.e. the SoC of the energy storage system, is estimated based on the DC-link voltage, assuming a bijective function linking these two values. This estimated SoC is compared to reference values to compute the error signal of two PI controllers the role of which is respectively to define the set-point for the power extracted from or injected into the AC grid. This estimation of the SoC is also compared to a third reference value in order to determine the state of the flexible loads.

These reference values can be fixed and predefined, during the system design for example, or continuously optimized based on previsions of the local production and consumption. These operations would occur at the supervision level, as illustrated on Figure 13.

PI controllers for the different services
The different energy services mentioned in the introduction of this document (increased self-consumption, peak-shaving and ramp-rate limitation) are provided through the adequate use of the two PI controllers illustrated on Figure 13. More details are given below for each of these services.

Self-consumption
The increased self-consumption is achieved by the use of unidirectional PI controllers with clearly separated reference values. One of the PI controller can only impose a positive reference value for the power exchanged with the grid i.e., a power extracted from the grid. Its reference SoC value, E_2, is lower than the reference value E_4, of the second PI controller that can only impose a negative reference value i.e., a power injected to the grid.

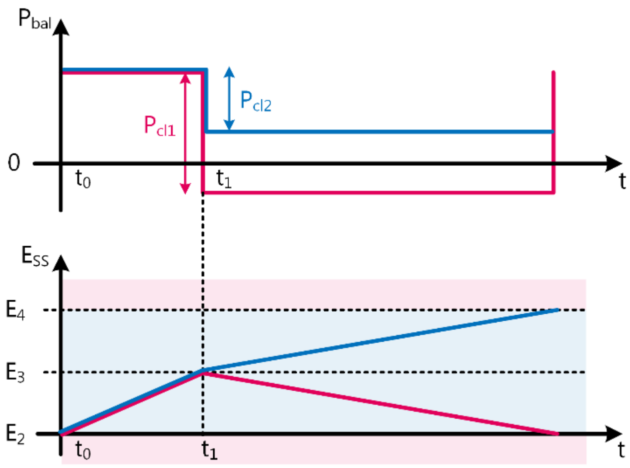

Figure 14: Evolution of the power balance and the battery state of charge in two scenarios

Between these two thresholds, no power is exchanged with the grid and the ESS SoC evolution depends on the internal power balance, as schematically illustrated on Figure 14.

If the local production exceeds the local consumption, the excess energy is stored in the Energy Storage System until this SoC reaches E_4 and the corresponding PI starts to inject the excess power into the grid to stabilize the SoC at its reference value. On the other hand, if the local consumption exceeds the local production, the required additional energy is taken out of the ESS, making its SoC decrease until the E_2 threshold is reached and the corresponding PI controller starts to take power from the grid to stabilize the SoC at this reference value.

Therefore, the energy storage capacity corresponding to the difference between these two thresholds is used to increase the self-consumption since it is used to momentarily store excess energy production in order to use it later when the local production is not enough to entirely supply the local consumption.

Peak shaving
The same PI controllers can also be used to provide the peak-shaving service, both for the power extracted from the grid and for the power injected into it. This is achieved by setting a limitation to the

power reference value that is computed by the PI controllers. Figure 15 illustrates this behaviour for a limited injected power.

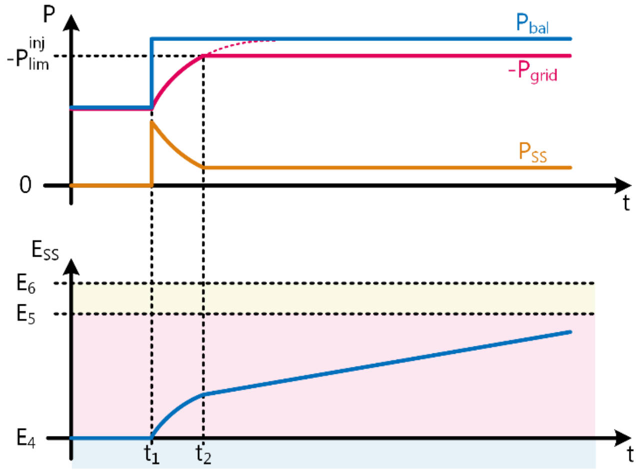

Figure 15: Evolution of the net power consumption (P_{bal}), the power exchanged with the grid (P_{grid}), the charge/discharge power of the battery system (P_{SS}), and the state of charge of the storage system (E_{SS}) illustrating peak-shaving for the injected power.

Once the SoC is stabilized at E_4, if the local production still increases so that the power balance exceeds the set limitation, the reference value for the injected power will be limited and the remaining excess power will be then be stored in the ESS. For security reasons, this limitation is disabled when the SoC reaches the E_5 threshold. Thus, the energy storage capacity corresponding to the difference between E_4 and E_5 is used to provide the peak-shaving service. A similar reasoning can be done for the power extracted from the grid. In such a case, the corresponding storage capacity will be the one between E_1 and E_2.

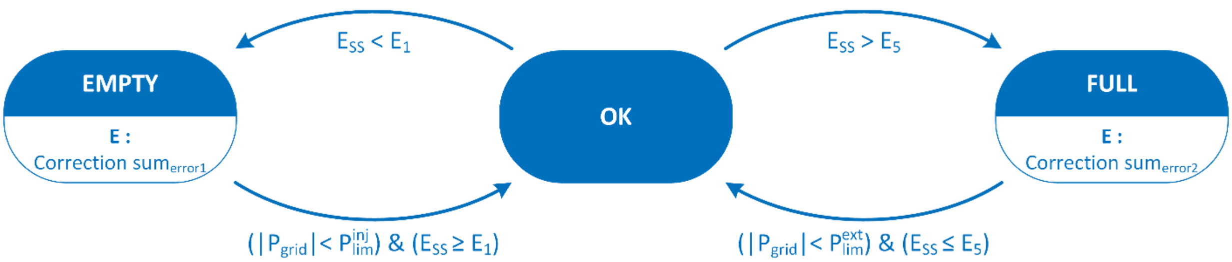

Figure 16: State machine controlling the peak-power limitation, which is activated when the system is in the central ("OK") state.

The power limitation can be disabled when the SoC reaches the E_1 and E_5 thresholds, respectively to avoid an excess charging and excess discharging of the energy storage system, as summarized on Figure 16.

In order to avoid a ringing phenomenon between the states where the power limitation is disabled and enabled, a second condition is added on the grid power reference value. This reference value must be, in absolute value, less than the limitation.

Moreover, it must also be noted that an artificial correction is performed on the PI controller internal state, the cumulated error, when the power limitation is disabled. This corrections allows to ensure a continuity in the power reference value computed by the PI controller.

Ramp-rate limitation

The last service, the ramp-rate limitation, is also performed thanks to the use of the PI controllers. More precisely, this service is achieved through the definition of the closed-loop equivalent time constant. Indeed, it can be mathematically demonstrated that the time constant characterizing the response of the PI controller to a perturbation is the same that the time constant characterizing the response of the system to a change of reference value.

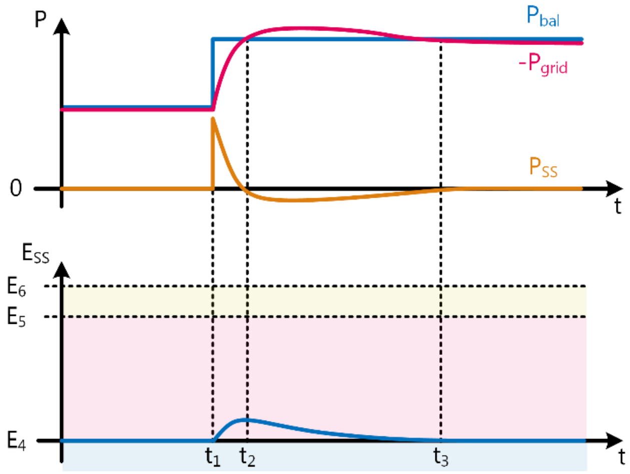

Figure 17: Evolution of the net power consumption (P_{bal}), the power exchanged with the grid (P_{grid}), the charge/discahrge power of the battery system (P_{ss}), and the state of charge of the storage system (E_{ss}) illustrating the limitation of grid power variations.

Figure 17 illustrates the limitation of the variation of grid power compared to the variation of the perturbation, here a suddenly increasing local production when the SoC is stabilized at E_4. In such a case, the sudden increase in the power balance will lead to an increasing SoC, thus creating an error from the PI controller point of view. The controller will react to this error and increase the power injected into the grid to bring the SoC back to its reference value. Nevertheless, the controller reacts with a limited and predefined bandwidth and therefore acts as a low-pass filter, effectively limiting the variation of the power exchanges with the grid. Such a behaviour is made possible by the fact that, during the transient, the power difference is assumed by the energy storage system, as depicted in orange on Figure 17, and lead to a transient increase of the SoC, reaching its maximum at $t=t_2$ on the considered figure. This maximal value is directly linked to the controller bandwidth and the magnitude of the perturbation. Thus, a security margin must be kept regarding the maximum and minimum allowed SoC. On Figure 17, this margin corresponds to the energy storage capacity located between E_5 and E_6. A similar reasoning can be made on the low-SoC side of the energy storage, with a security margin located between E_0 and E_1.

As previously mentioned, it can be demonstrated that the limitation of the ramp-rate is defined by the closed-loop bandwidth of the SoC control through the PI controller. This controller can be designed through the loop-shaping approach illustrated on Figure 18.

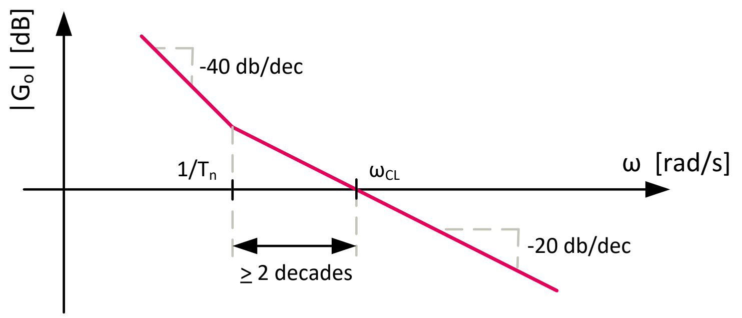

Figure 18: Sizing of the PI controller for a given closed-loop bandwidth

PI parameters T_n and T_i are adjusted such that the open-loop transfer function, given by the product of the transfer function of the controller and of the system, a pure integrator in the considered case, crosses the 0db line at a pulsation ω_{cl} corresponding to the desired dynamic. Moreover, the change of slope, from -20db/decade to -40 db/decade must occur at least two decades away from the crossing of the 0db line.

Such a sizing of the PI controllers ensure a behaviour close enough to the first-order low-pass filter approximation mentioned above. It must be mentioned here that the two PI controllers can be sized with different bandwidth if the distinct dynamic behaviours are wished for the injected and extracted power.

Virtual splitting of the storage capacity

These considerations on the link between the different energy services and the parts of the energy storage capacity they use can be summarized according to Figure 19.

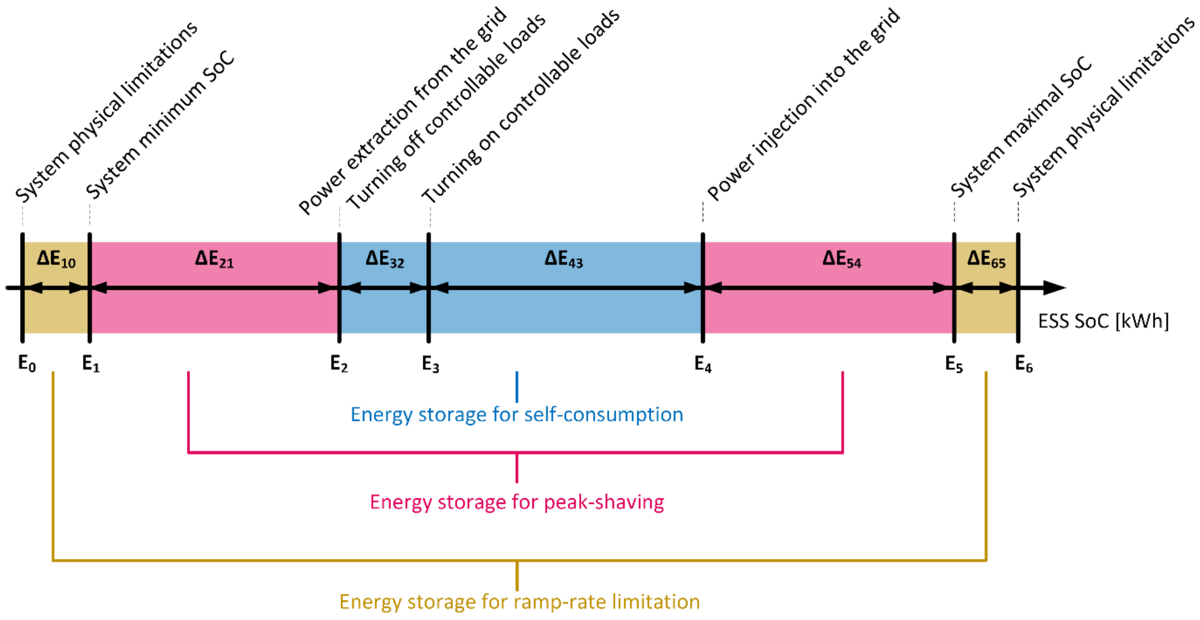

Figure 19: Allocation of storage capacity to the different services

The coloured areas correspond to the different energy services: yellow for the ramp-rate limitation, red for the peak-shaving and blue for the increased self-consumption. This last area includes an additional threshold, E_3, linked to the use of flexible loads. If the SoC reaches this value, the flexible loads will be turned on in order to increase the local consumption in order to bring the SoC back to E_2. In order to avoid ringing phenomena, a hysteresis is introduced and these flexible loads will not be turned off before the SoC reaches the lower bound of the area dedicated to self-consumption, namely E_2.

It must also be noted that ramp-rate limitation is also performed in the red areas. This detail is not mentioned on Figure 19 for the sake of simplicity.

Energy storage sizing tool

The control strategy being defined, the behaviour of the closed-loop system can be studied in order to assess the energy storage capacity required to reach predefined objectives. This section is organized according to the different services provided by the micro-grid, namely the increased self-consumption, the ramp-rate alleviation and the peak-shaving.

Ramp-rate control

The yellow areas of Figure 19, dedicated to ramp-rate control, have to be considered as security margins against SoC overshoots due to perturbations on the power balance and the limited bandwidth of the PI controllers, as illustrated on Figure 20.

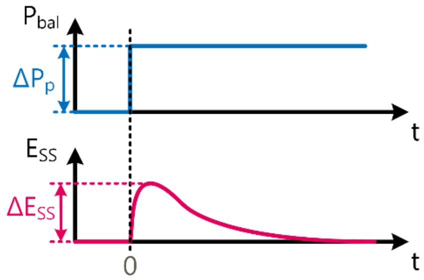

Figure 20: SoC overshoot due to perturbations

The sizing of ΔE_{10} and ΔE_{65} is based on a worst case scenario. An infinitely fast change of the power balance of a magnitude ΔP_p is considered. Then, from the system closed-loop transfer function and an inverse Laplace transform, it is possible to analytically express the time evolution of the stored energy as follows, where A and B are coefficients related to the closed-loop equivalent time constant and s_1 and s_2 the associated poles.

$$E_{ss}(t) = (A * e^{s_1 t} + B * e^{s_2 t}) * \Delta P_p + E_{ss}(t=0) \quad (2)$$

The maximum value of E_{ss} is reached at $t=t_{max}$, given by the following equation.

$$t_{max} = \frac{\ln(s_1) - \ln(s_2)}{s_1 - s_2} \quad (3)$$

Thus, the energy overshoot ΔE_{ss} is defined as:

$$\Delta E_{ss} = (A * e^{s_1 t_{max}} + B * e^{s_2 t_{max}}) * \Delta P_p \quad (4)$$

Intervals ΔE_{10} and ΔE_{65} are sized to ensure that, in case of a perturbation of a magnitude ΔP_p, here selected as half the operating range, the energy stored in the storage system never exceeds the operating range.

Self-consumption and peak-shaving

By opposition to the two previously mentioned cases, the overall system behaviour cannot be studied analytically. Therefore, the sizing of the remaining intervals, namely ΔE_{21}, ΔE_{43}, and ΔE_{54}, is achieved through model-based simulations, as illustrated on Figure 21.

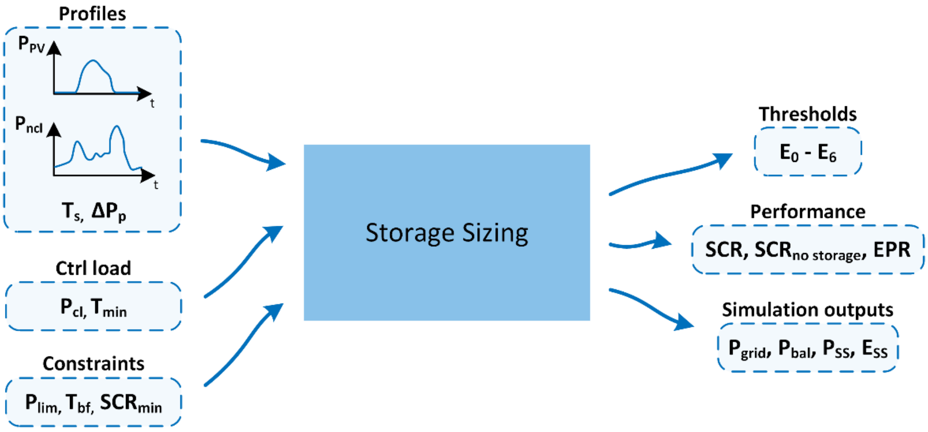

Figure 21: Working principle of the ESS sizing tool

Production and consumption profiles are fed to the model, alongside parameters such as the rated power of the flexible loads and the associated minimal cycle period and constraints linked to the performance objectives, such as the power limitation, the closed-loop equivalent time constant defining the ramp-rate alleviation and the minimal acceptable self-consumption ratio SCR_{min}.

The control thresholds E_0 to E_6 are then iteratively adjusted until the specified performances are met. The achieved self-consumption ratio is compared to the one that would have been achieved in the absence of any energy storage system. The Energy to Power Ratio (EPR) is also computed in order to determine the most suitable energy storage technology. Finally, the different relevant power profiles are computed for representation purposes.

Simulation results

Illustrations of the model and sizing tool possible outcomes are given in this section. Figure 22 shows the results of a day simulation using a reference balance power profile P_{bal}. The related simulation parameters and sizing objectives are summarized in Table 3.

Table 3: Simulation parameters

Maximal perturbation	Flex. loads rated power	Flex. load min. cycle time
ΔPp = 10 kW	Pcl = 1 kW	Tmin = 10 minutes
Grid power limitations	**Min. self-consumption**	**Ramp-rate control equivalent time**
Pmax = 5 kW	SCRmin = 70%	Tbf = 30 sec

The upper part of Figure 22 shows the day profile of the power exchanged with the upstream AC grid. One can observe both the reduction of the time variations and the respect of the maximal injection and extraction values P_{lim}^{ext} and P_{lim}^{inj}.

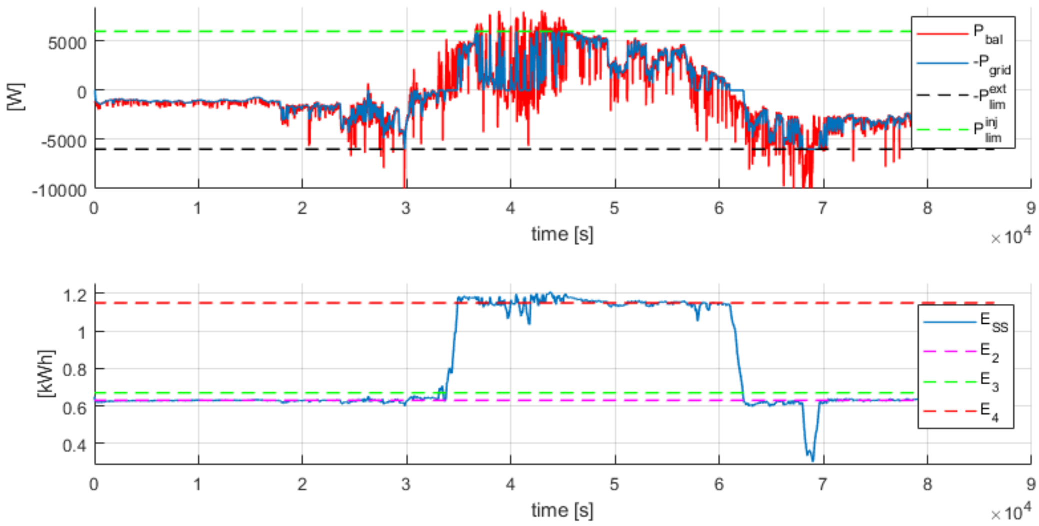

Figure 22: Power and ESS SoC profiles

The lower part of the same figure shows the corresponding evolution of the energy stored in the ESS. The computed control thresholds are represented on Figure 23 in reference to Figure 19.

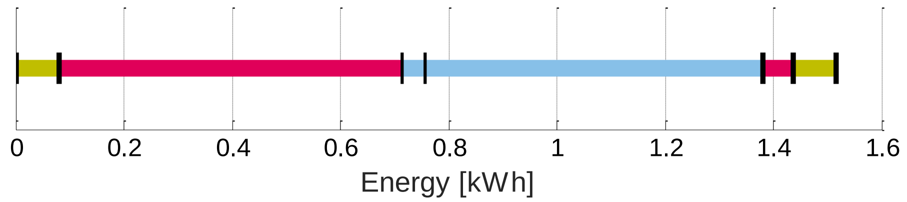

Figure 23: Sizing tool results

Control strategy: practical implementation

While the control strategy described in the previous section has been validated in simulation, its practical translation on a physical system has required additional developments to account for the limitations of the hardware components.

Overcurrent protection for battery

Since the peak power of the PV installation is higher than the power capacity of the battery, a battery power limitation had to be implemented to avoid excess battery current when the PV production is high and the load consumption low. The same issue can occur the other way around, in case of high load consumption and low PV production.

Indeed, since the battery converter is regulating the DC bus voltage, it is completely transparent in terms of power flow. The powers flowing inside the DC grid are a result of the balance between production and consumption, and the controlled grid power.

To avoid reaching the battery physical power capacity, an additional protection controller was developed. For that purpose, a correction factor of the grid controlled power is generated by a set of two PI controllers. The topology of the controller is presented in Figure 24.

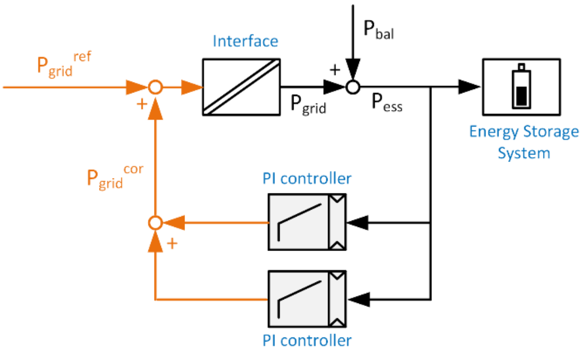

Figure 24: Protection controller to prevent battery overcurrent in charge or discharge.

In this topology, one PI controller is dedicated to limiting the battery charging current and the other is dedicated to limit the discharging one. Both include output saturation in order to avoid cross interference. The tuning of the controller has been done following the Ziegler–Nichols method.

In Figure 25, measurements of the power limitation of the charging controller is illustrated. This represents a situation with high PV production and no load consumption. The SoC being in the "self-consumption area", the grid power is supposed to be zero. However, since the power balance is exceeding the maximum power capacity of the battery (3.6 kW), this power is limited by injecting the excess in the grid.

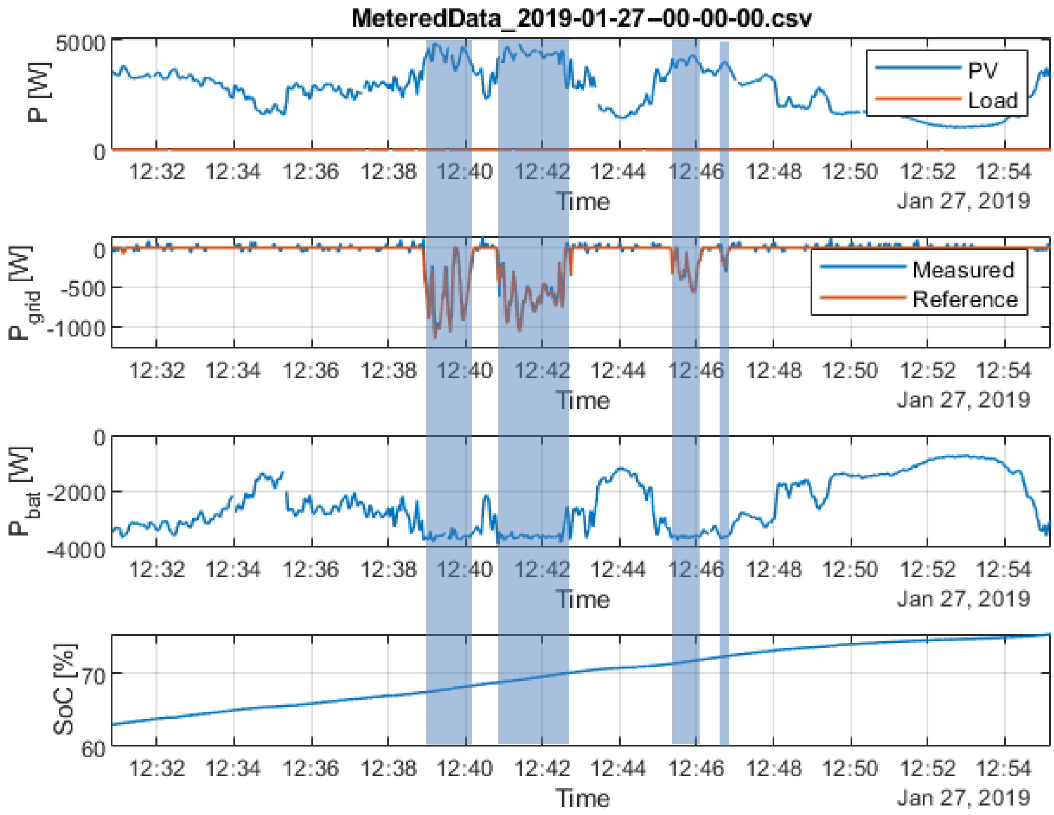

Figure 25: Evolution of PV generation, load, grid and battery power and battery SoC in a situation of high power imbalance where the battery charging power reaches its upper limit (blue highlights).

DC bus voltage regulation

In our control architecture the DC bus voltage, regulated by the battery converter, is set proportional the battery SoC (see Figure 26).

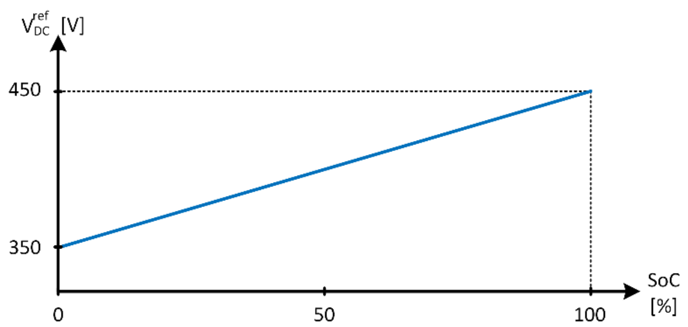

Figure 26: Relation between the reference voltage on the DC bus and the state of charge of the battery.

However, when testing the system in the laboratory prior to its installation on site, we observed that the converter was unable to properly regulate the DC voltage when charging or discharging the charg-ing. When the battery was charging the DC bus voltage increased above the set-point, and when it was discharging the DC bus voltage decreased below the set-point.

The reason for this unwanted behaviour is that the device-level current controller of the DC/DC bidirectional converter is a proportional controller (Figure 27). Therefore, a current is flowing into/from the battery only when an error between the DC bus voltage reference (V_{DC}^{ref}) and the measured one (V_{DC}^{meas}) is observed.

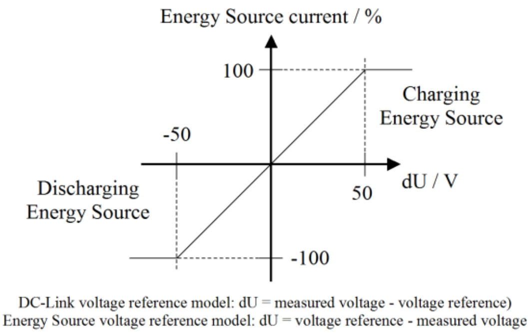

Figure 27: Device-level control of the DC/DC bidirectional converter (source: MSc Electronics Oy)

To work around this limitation, we developed an additional PI controller which determines an offset to be applied on the set-point for the DC bus voltage (Figure 28)

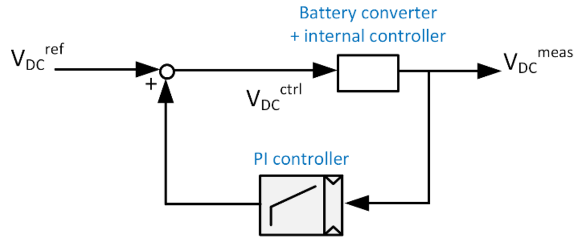

Figure 28: Additional PI controller to compensate the limitations of the battery converter.

With this correction, a regulation of the voltage can be achieved (Figure 29). In this experiment, the grid converter was controlled in order to charge and discharge the battery with a varying power.

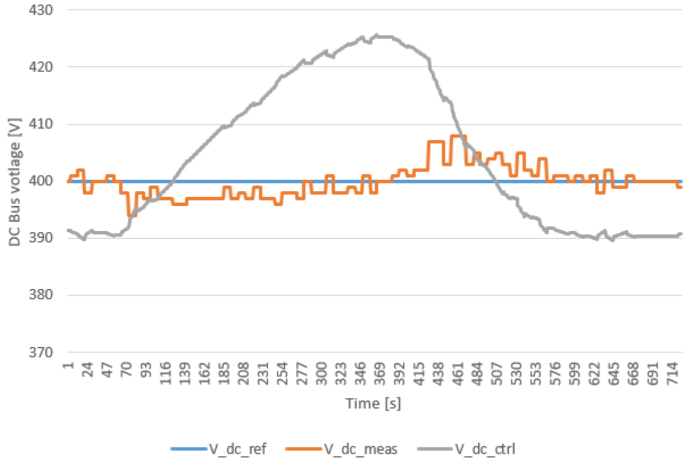

Figure 29: Validation of the additional PI controller; evolution of the "true" reference voltage for the bus (V_dc_bus), of the corrected reference voltage provided to the battery converter (V_dc_ctrl), and of the measured voltage on the DC bus (V_dc_meas).

SoC resolution issue
In the first laboratory tests, we observed extremely large set-points for the grid power when the battery SoC reached “peak-shaving areas” (E_2 or E_4 thresholds).

The reason for that behaviour turned out to be an excessive discretisation of the battery SoC, which is the main input for the control. Indeed the battery management system (BMS) of the BYD battery provides the SoC with a resolution of 1 percentage point. As a result, the minimum non-zero error on seen by the PI controllers is 1% of the full capacity, which results in a huge control signal. Therefore a higher SoC resolution is needed in order to have a smooth control of the grid power set-point.

The solution we implemented was to use the information of battery current and voltage provided by the BMS to compute the SoC with a higher resolution. The battery power ($P_{bat} = V_{bat} \times I_{bat}$) is integrated and scaled by a factor K calculated experimentally ($\Delta SoC = \int_t KP_{bat}dt$). This integration is used to compute the fractional part of the SoC to the second decimal, and is limited to [0.00 – 0.99]. As soon as the value provided by the BMS is updated, the fraction part is set to either 0.00 (if BMS SoC increases), or 0.99 (if BMS SoC decreases).

This approach was experimentally validated (Figure 29); SoC values provided by our estimator are in good agreement with those provided by the BMS at each refresh.

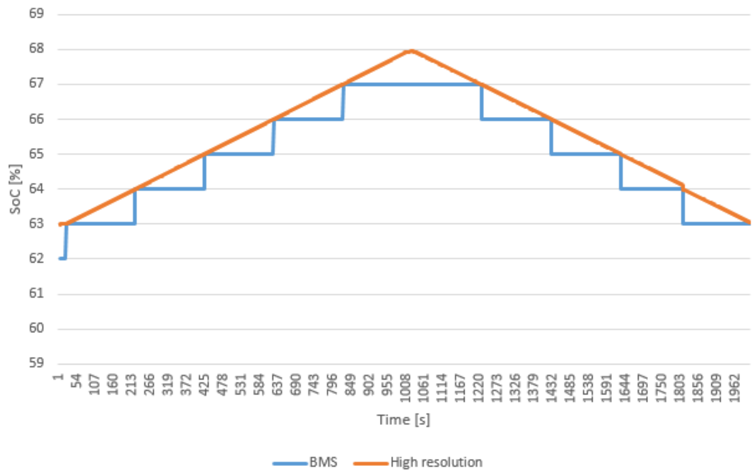

Figure 30: Evolution of the SoC provided by the BMS (blue) and corrected by integrating the battery power (orange) during a charge/discharge partial cycle at constant current.

Swiss demonstrator

Data acquisition
Figure 31 illustrates the different data flows in the Swiss Demonstrator.

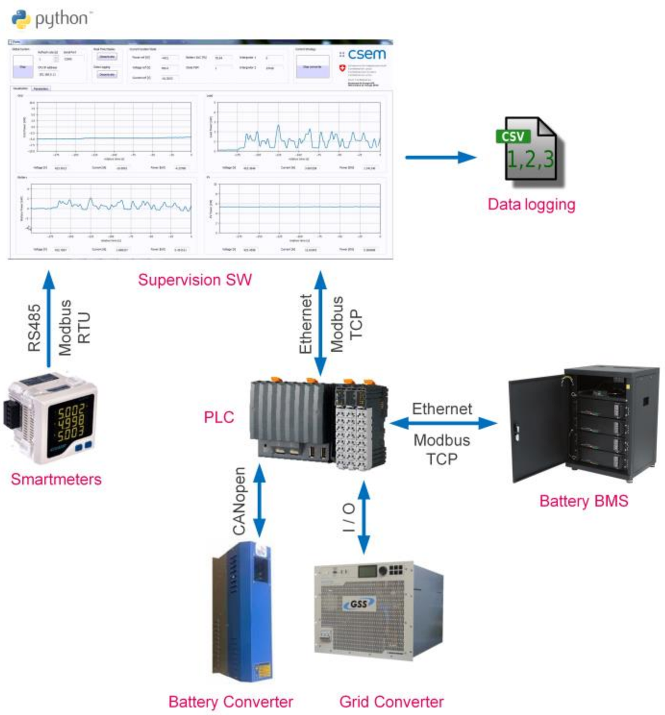

Figure 31: Data flows in the Swiss demonstrator.

All the power flows are measured by dedicated DC smart meters. These smart meters are interfaced with the central control unit, implemented on an industrial PC, through an RS-485 bus supporting a ModBus RTU communication protocol. These measurements are used only for monitoring purpose. They can be graphically displayed to the user and/or logged for further analysis with a refresh rate down to 1 second. Through this user interface (Figure 32), the user can:

- Launch the supervision system
- Start and stop the bidirectional AC/DC converter
- Monitor the state of the system: battery state of charge, set-points, internal variable of the controllers
- Visualise the temporal evolution of power flows (grid exchange, load consumption, battery charge and discharge, PV production).

For monitoring purposes it is crucial to have a reliable data collection. At first electromagnetic compatibility issues with the battery converter created significant data loss. After modification to the cables and their layout, this issue was solved and data availability is now 99.9% with a sampling rate of 1 s.

Figure 32: Screenshot of the graphical user interface of the Swiss demonstrator.

On-site testing protocol

The demonstrator has been running on the Swiss site since December 2018. Since the loads follow an industrial schedule their profile has little day-to-day variability. Results can therefore be observed over a few days without loss of generality. Those presented in this section where acquired from the 25th to 27th January 2019. In that period the load had a square profile with 5 min, 1.8 kW spikes every 105 min.

High-level parameters for the control strategy were (Figure 33):

– E_2 = 40%

– E_4 = 80%

– $P_{lim,inj}$ = 4kW

– $P_{lim,ext}$ = 1kW / 3kW

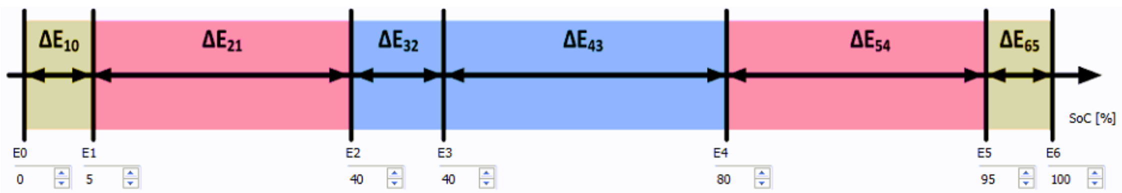

Figure 33: Distribution of the storage capacity and threshold levels applied in the period 25th to 27th January.

Results and discussions

Overview of performance over one day

Figure 34 shows the evolution of power flows and battery SoC over a 24 h period, with the battery starting with a 50% state of charge. On that scale, the observations one can draw are:

1. The system is capable of smooth, continuous operation
2. The battery system is effectively used between 40% and 80% of its capacity to increase self-consumption by storing excess PV electricity and powering the loads.

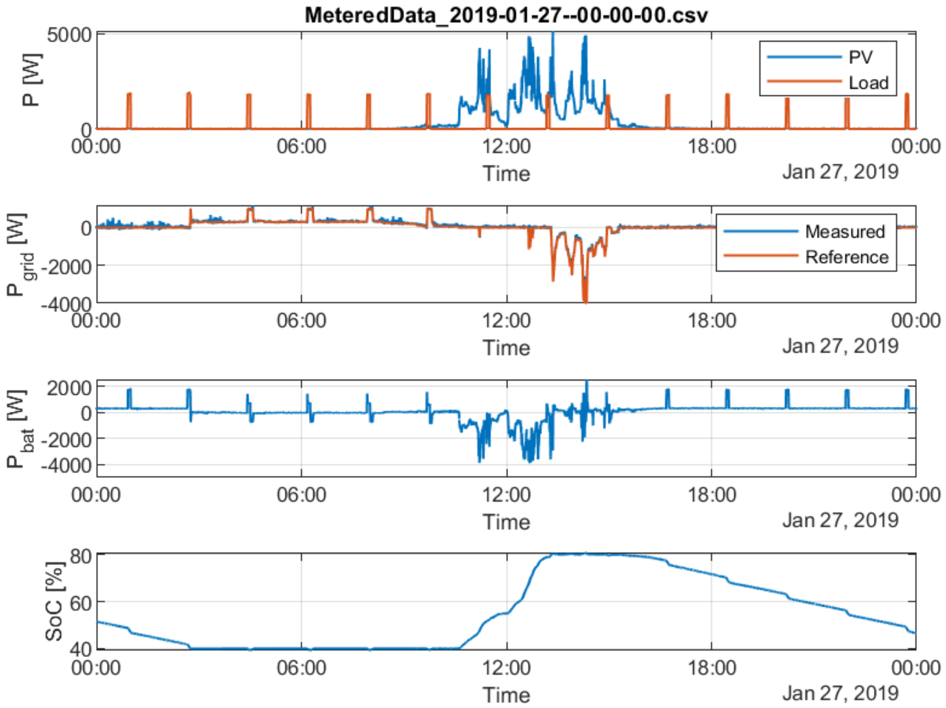

Figure 34: Evolution of PV generation, load, grid and battery power and battery SoC over 24 h.

The subsequent sections focus on validating individual parts of the control strategy.

Validation of self-consumption

E2 (40% SoC)

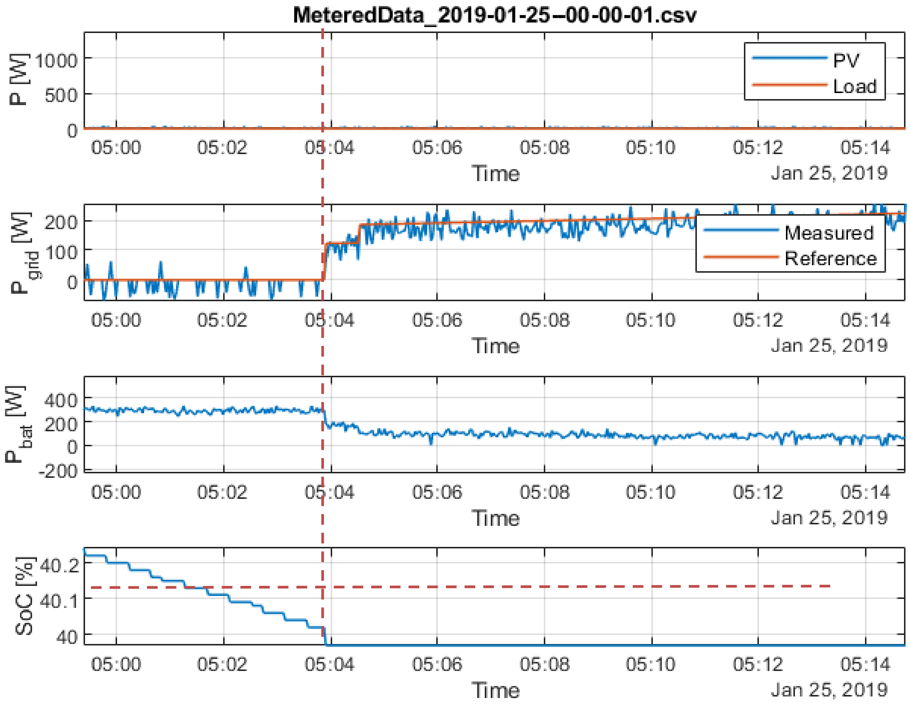

Figure 35: Evolution of power flows and SoC in the demonstrator shortly before and after the system reaching threshold E2 (40% SoC, 05:04).

Figure 35 validates the state transition in the system when it reaches threshold E2 (lower bound of the self-consumption range): at that stage the power drawn from the grid becomes non-zero and the battery power decreases.

E4 (80% SoC)

Symmetrically, Figure 36 validates the state transition in the system when it reaches threshold E4 (upper bound of the self-consumption range): at that stage the microgrid starts injecting power into the grid and the battery charge power decreases. On this graph the ramp-rate limitation is already clearly visible, since the transition from 0 to full PV power for the grid converter takes about 2 min 30 s.

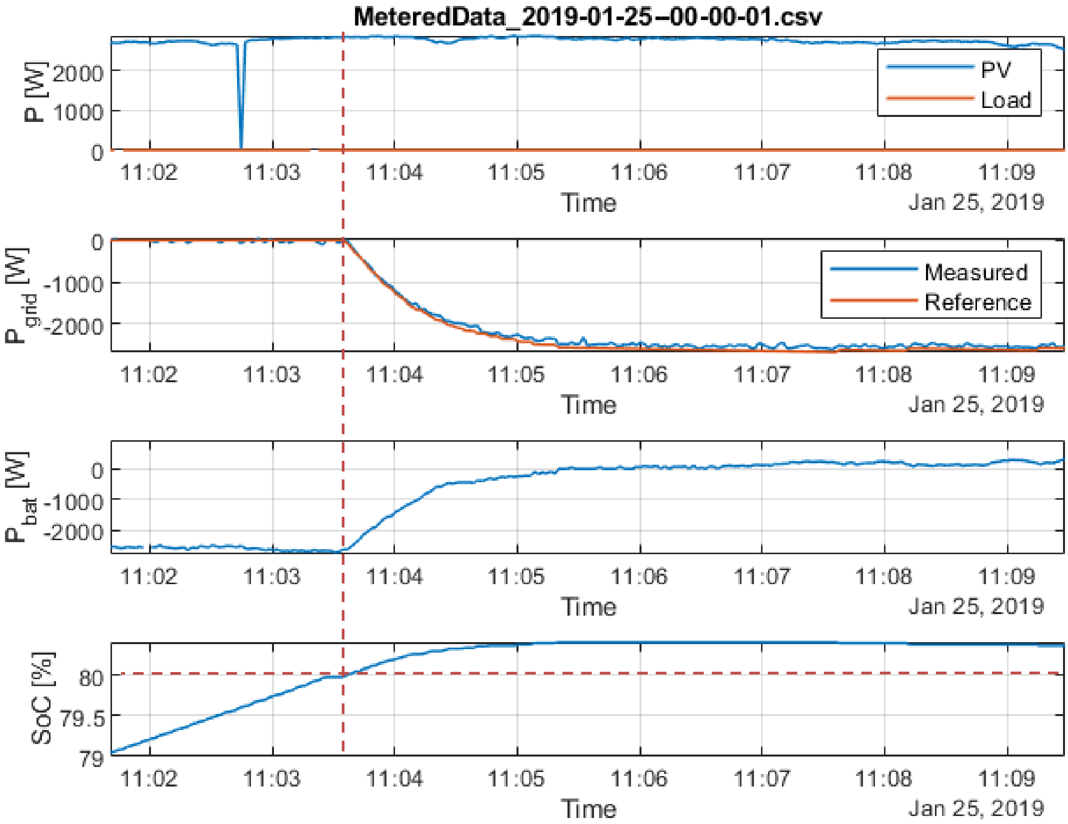

Figure 36: Evolution of power flows and SoC in the demonstrator shortly before and after the sys-tem reaching threshold E4 (80% SoC, 11:03:30).

Validation of ramp-rate control

For the validation of ramp-rate control the maximum power from the grid was set at a relatively high value (3 kW, vs. a peak power consumption of 1.8 kW). This way, the peak-shaving mode was never activated during the day, thereby isolating the ramp-rate control.

The results, illustrated on Figure 37, are in line with the expected and simulated behaviour of the sys-tem: the grid power varies smoothly and on a much longer timescale than the load (2 min 30 s to reach a new steady-state value), at the expense of the state of charge of the battery being outside the self-consumption range for a short period of time.

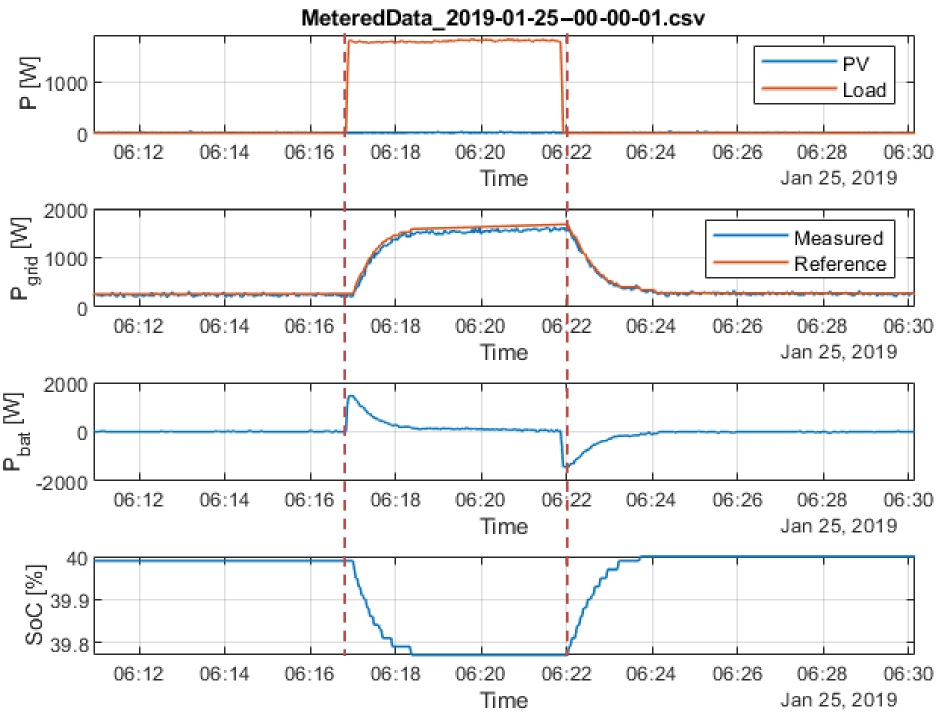

Figure 37: Evolution of power flows and SoC in the demonstrator shortly before a step increase (at about 06:16:30) and after a step decrease (at about 06:22:00) in power consumption from the load.

Validation of peak shaving

Power drawn from the grid

For that experiment the maximum power drawn from the grid was set at a low value (1 kW vs. a peak power consumption of 1.8 kW) on the power exchanged with the grid.

The results, shown on Figure 38, match the expectations and the simulations: the power from the grid slowly increased until reaching its limit value, the battery SoC went relatively far from the E2 threshold into the peak-shaving range, and it went back to this threshold after the peak-shaving event.

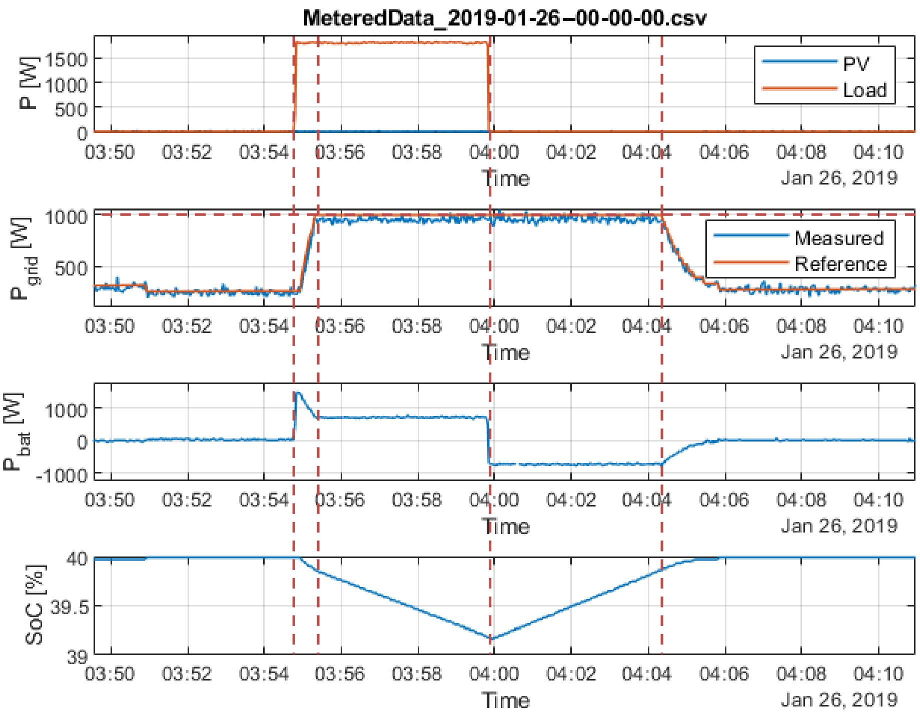

Figure 38: Evolution of power flows and battery SoC around a peak consumption event (03:54:30 to 04:00:00). When the power consumption peak starts (first vertical dashed line), the battery discharge current shoots up; in parallel, the power drawn from the grid increases only slowly due to the ramp-rate limitation mechanism. When it reaches its upper limit (here set a 1 kW, horizontal dashed line) it saturates and the battery keeps discharging to make up for the difference between the limit and the actual power consumption. When the power consumption from the load drops (third vertical dashed line) the power drawn from the grid remains constant while the battery recharges to get back near the E2 threshold. From the fourth vertical dashed line onwards the power drawn from the grid slowly decreases so that it becomes zero when the state of charge reaches the E2 threshold (lower bound of the self-consumption range) again.

Power injection into the grid

That validation can only be conducted on a day of relatively high PV production. In that case, the limit for power injection was set at 4 kW i.e., about half the peak power capacity of the PV system.

The results are shown on Figure 39 and validate the expected behaviour. Indeed, the injected power into the grid saturated at the set limit value of 4 kW. In addition, the smoothing effect of the ramp-rate control mechanism is visible both before the peak production, when the PV output showed rapid fluctuations, and after, when the injected power slowly went down to the new, near-steady-state value of about 1.2 kW. Finally, the battery SoC went significantly above the E4 threshold (upper bound of the self-consumption range) during the peak, well into the peak-shaving range, and went back to E4 after the peak production event.

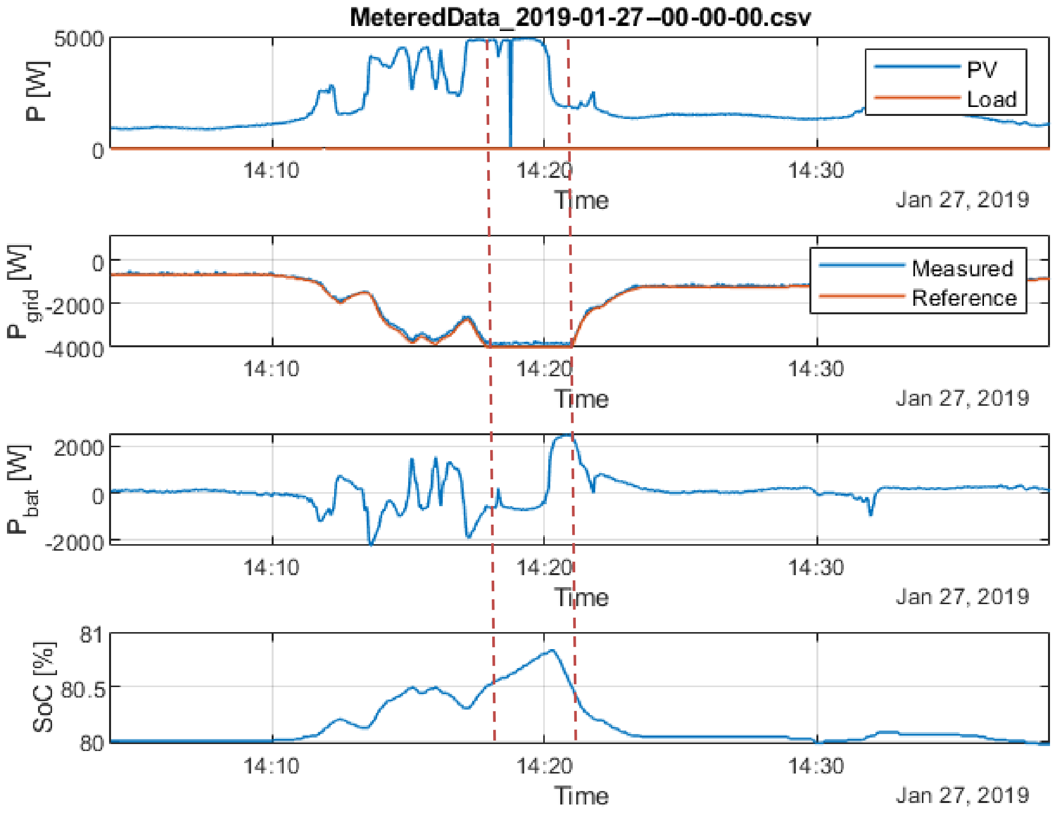

Figure 39: Evolution of power flows and battery SoC around a peak injection event. In the section before the first vertical dashed line, the battery SoC increases beyond the E4 value (upper bound of the self-consumption range) as it is used to filter out the rapid fluctuations in PV power production from the power injected into the grid. Between the two vertical dashed lines the power injection into the grid is at its maximum value; the battery first absorbs the excess PV production, then discharges after the peak production to go back towards the E4 threshold (upper bound of the self-consumption range).

Remaining challenges

While the main features of the control strategies have all been experimentally validated, a few technical challenges remain which ideally would be solved in a commercial product.

Instability at low PV production

When the PV power production is very low (between 0 W and 200 W) the output of the string optimizer is unstable and switches off from time to time (Figure 40). This behaviour, which is common to all PV converters, creates some stress on the battery converter. Indeed, that converter produces audible oscillations at frequencies between 2 Hz and 4 Hz.

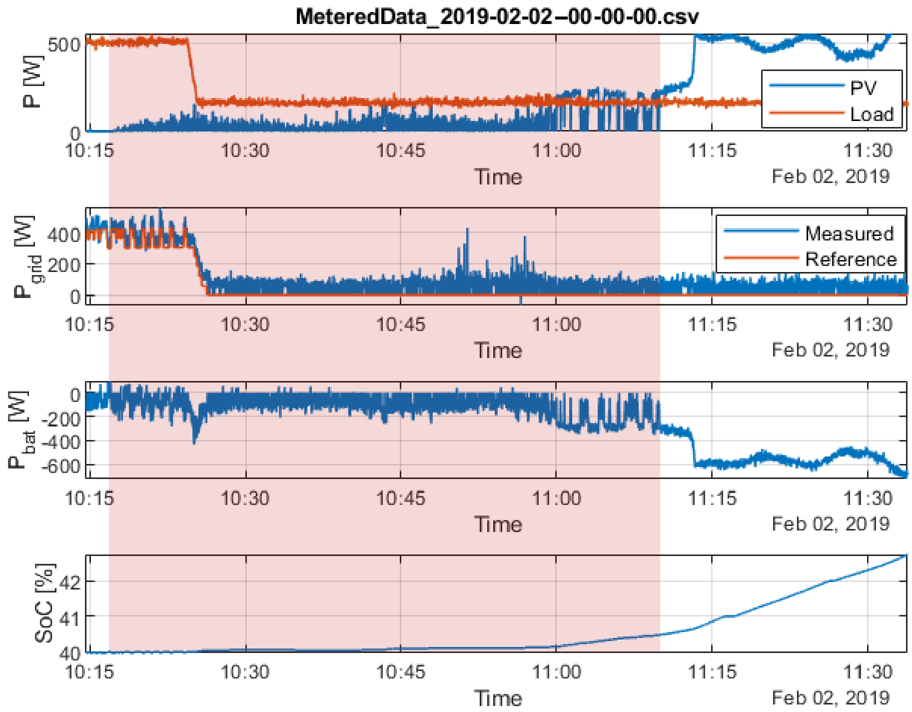

Figure 40: Rapid oscillations in power due to the string optimizer at very low PV power.

Oscillations at the E2 threshold

As shown on Figure 41, when the balance between production and consumption is constant and small and the battery is close to the boundary between two states of the system (in this case, close to the lower boundary of the self-consumption range, E2=40%), the power flows to the grid and the battery oscillate periodically. These oscillations, whose amplitude is small, are due to the discretisation of the battery SoC, which is an input to PI controllers.

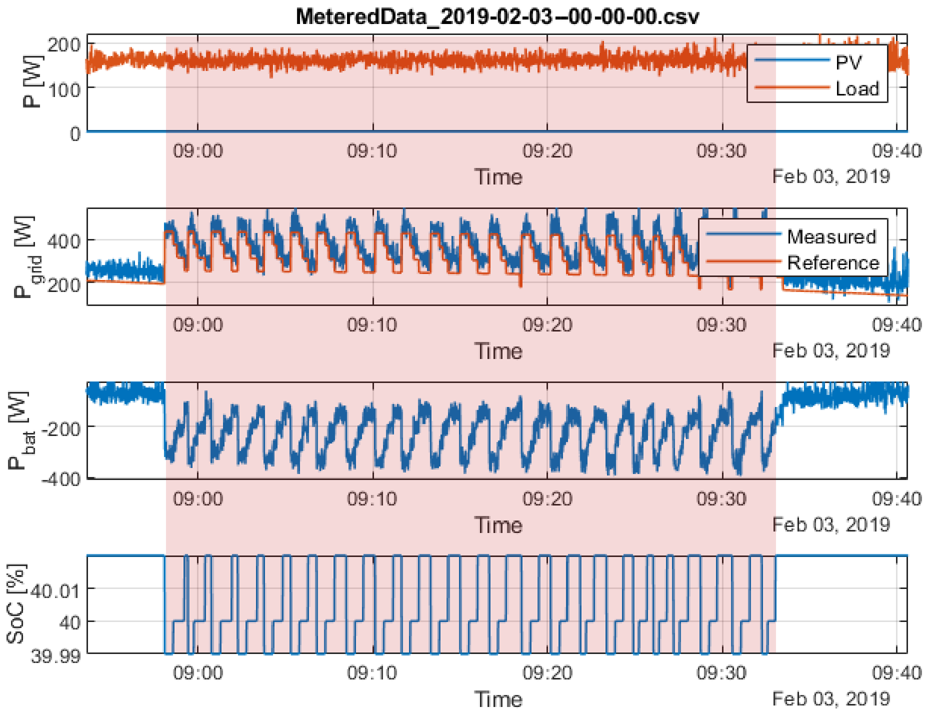

Figure 41: Oscillations in power at constant load when the battery SoC is close to threshold E2 (here: 40%)

Standby energy consumption

During the night, in the absence of PV production, the system is powered by the battery as long as its state of charge remains in the self-consumption range. When the load is also zero during the night, as is the case on Figure 42, the observed power consumption comes from the power conversion and distribution system itself. In such a situation, the decrease in SoC is 23 percentage point in 14 h. This corresponds to an energy consumption of 1.2 kWh and a continuous, standby power consumption of 84 W. The main source of this standby power consumption is the battery converter. Indeed, since it controls the DC bus voltage, it cannot be turned off at any time.

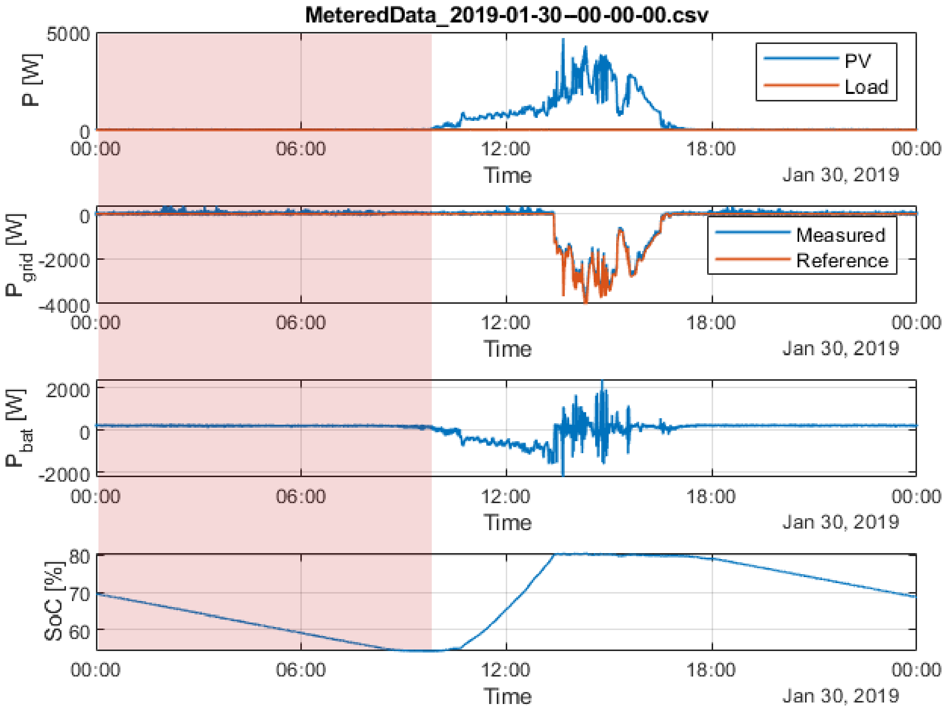

Figure 42: Evolution of power flows and battery SoC during the night, used to compute the standby losses of the system.

Economic analysis

Objective

The objective of this chapter is to perform an economic analysis of the DCSMART control strategy based on realistic scenarios. A comparison is made with a basic battery control strategy and with a system without storage. Moreover, the impact of the energy and power tariff and the type of load profile on the economic performance is assessed.

Benchmark

In order to obtain relevant results, the analysis is performed on 1 year of simulation, using 2 different purchase tariffs, 3 different feed-in tariffs, an optimally sized battery and optimized control parameters (i.e. thresholds and power limitation). The assessment is carried out on 3 different buildings with their specific load profile and yearly energy consumption. The irradiance profile used is the same for all buildings, only the nominal power of the PV installation is adapted.

In this assessment, the economic performance is evaluated using the overall operating cost. This overall operating cost includes the energy and power purchased cost, the feed-in retribution and the storage cost.

Profiles

The three types of evaluated building are: household, corporate offices and manufacturing industry. The detailed definition of each type and the source of the data are presented in the following list.

– **The household** consumption profile are generated with the tool LoadProfileGenerator[2] (LPG). This tools can produce yearly synthetic profiles with a resolution of 1 minute. The selected profile is from a household of type CHR44, according to LPG nomenclature, which corresponds to the consumption of a family of 2 adults and 2 children. The yearly energy consumption is of 3.35MWh. The daily superposition of the yearly profile is illustrated in Figure 43. It presents a typical domestic characteristic with high and short morning and evening peaks.

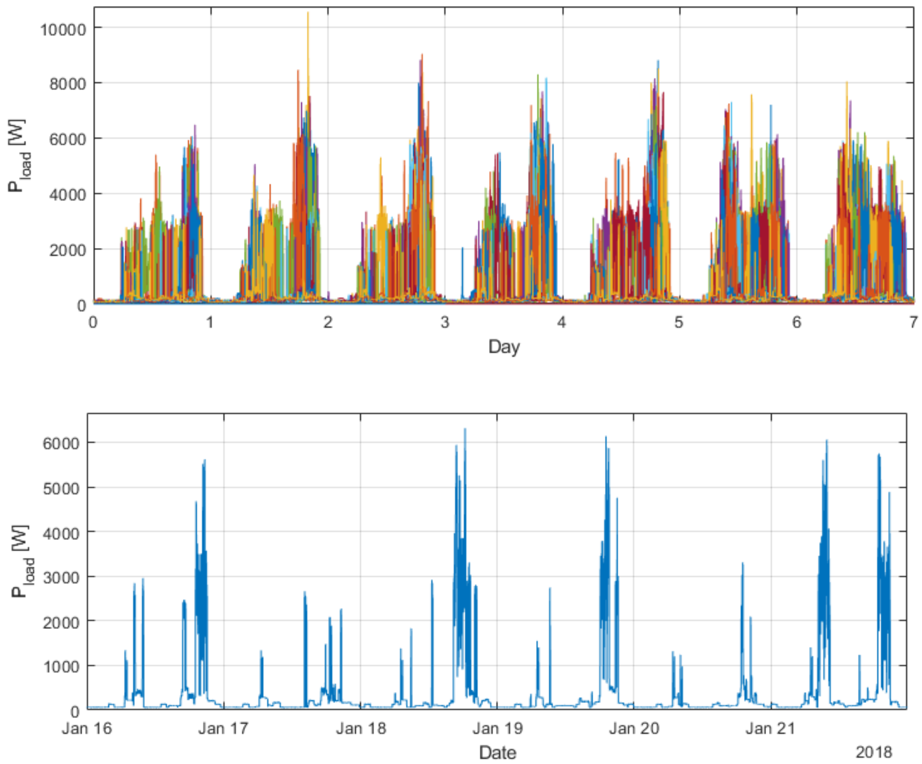

Figure 43: Weekly superposition of the yearly load profile (upper graph) and week example (lower graph) of a household (CHR44) generated by LPG

– **The corporate offices** consumption profile are measurement of a real offices building provided by EnerNOC Inc. through their Green Button Initiative Open Data Project [19]. The available dataset contains anonymized 5-minute energy usage data for 100 commercial/ industrial sites in the US for 2012. Site ID #9 of the dataset, which corresponds to corporate offices of 16'000m^2 located in New York, has been selected for the study. The yearly consumption of the building is 2.98GWh. These profiles are illustrated in Figure 44. A weekly pattern (with 5 working days) is clearly identifiable and the power consumption in the daytime is relatively constant.

[2] https://www.loadprofilegenerator.de/

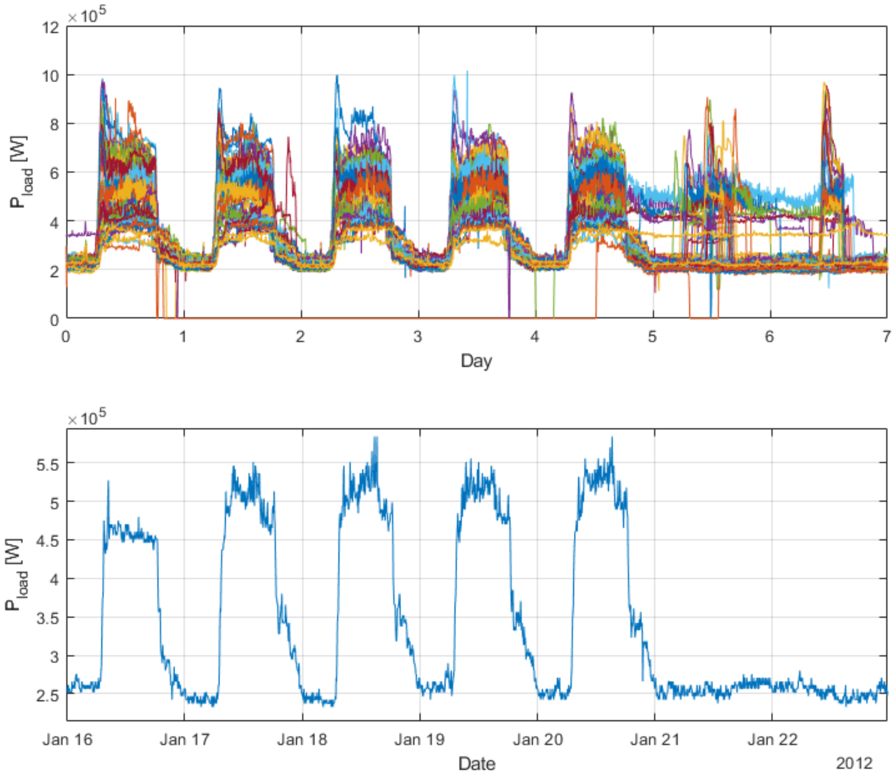

Figure 44: Weekly superposition of the yearly load profile (upper graph) and week example (lower graph) of the corporate office #9

– **The manufacturing industry** consumption profile from the same dataset as for the corporate offices. Site ID #761 of the dataset, which corresponds to an manufacturing industry of 12'000m² located in Chicago, has been selected for the study. The yearly consumption of the building is 3.02GWh. These profiles are illustrated in Figure 45. As for the previous example, a weekly pattern with 6 working days can be identified. However, while the yearly consumption is equivalent to the office building, the power consumption in the daylight is highly variable.

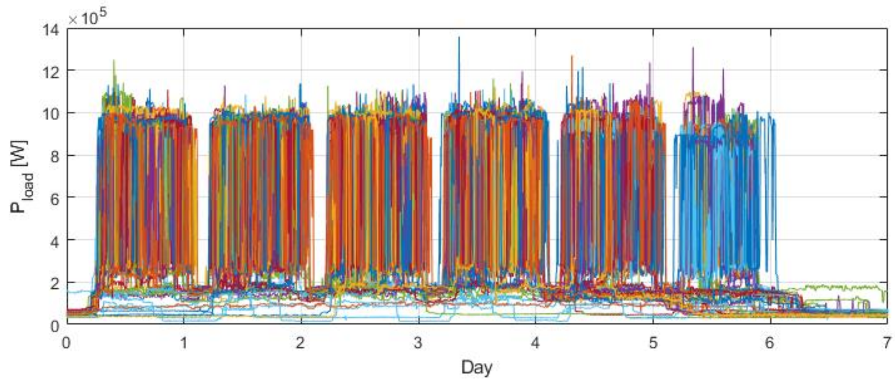

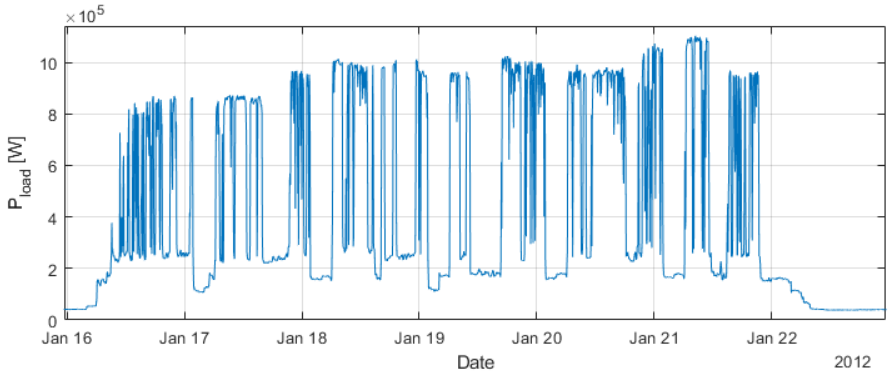

Figure 45: Weekly superposition of the yearly load profile (upper graph) and week example (lower graph) of the manufacturing industry #761

In order to compute the PV production profile, measurements of global horizontal irradiance (GHI) are used. These measurement have been acquired during year 2018 at CSEM's site in Neuchâtel with a 10 seconds resolution. In Figure 46 is presented the yearly GHI measurement profile as well as its superposed daily profile.

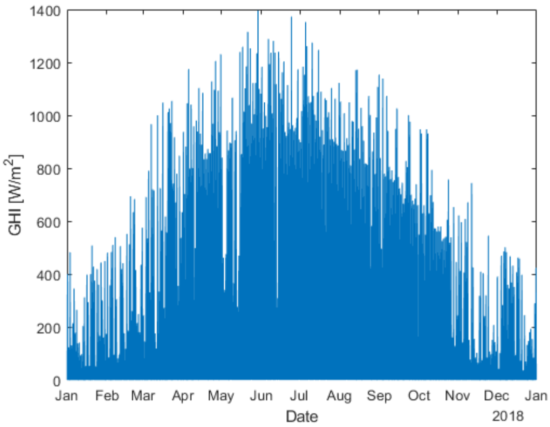

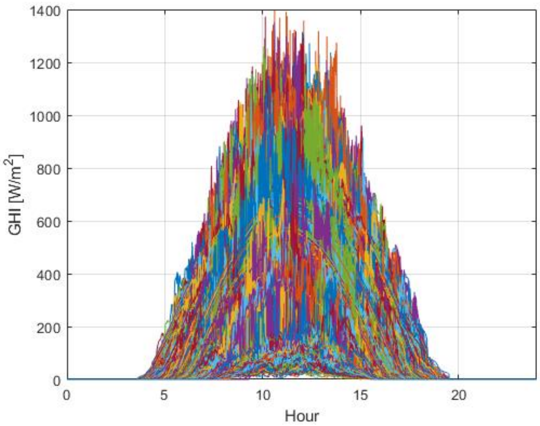

Figure 46: Yearly GHI profile (left) and its superposed daily profile (right) measured in Neuchâtel

The PV production is computed using a simple proportionality between GHI and installation peak power. Since the same GHI profile is used for all case studies, a scaled PV production profile will be associated to each of the presented building.

The scaling is performed in such a way that the yearly energy production meet a defined value. Regarding the yearly energy production of the domestic building, it is defined equal to the yearly energy consumption, thus 3.35MWh. For the office building, the assumption is made that 10% of its surface is covered by PV, with an estimated yearly performance of the PV installation of 190kWh/m^2, the yearly PV production is equal to 304MWh. Finally, it is assumed that 80% of the industrial building is covered by PV, thus a yearly production of 1'824MWh. A summary of the three evaluated buildings is presented in Table 4.

Table 4: Summary of the three evaluated buildings

Type	Surface [m^2]	Yearly consumption [MWh]	Yearly production [MWh]
Domestic	100	3.35	3.35
Corporate offices	16'000	2'980	304
Manufacturing industry	12'000	3'020	1'824

Tariff

As announced earlier, the economic assessment is performed using 2 different purchase electricity tariffs. The chosen tariffs are the one applied by Viteos AG in Neuchâtel for 2019[3]. Among the different rates proposed, the low voltage tariffs B2A and B2B will be evaluated for the domestic building. Regarding the industrial and office building, the medium voltage tariffs M1A and M1B will be compared.

All these tariffs include a power-related component (here, a fee charged each month based on the peak power used in that month). Although this component is rare in Switzerland for residential customers, it is common for commercial and industrial users. Power-related components for residential customers exist in Spain, Italy and Austria. Many distribution network operators see the introduction of power-related components in residential bills as a way to distribute infrastructure costs more fairly between prosumers and customers who cannot install PV.

In both cases, rates of type A emphasize the cost of the energy while rate of type B emphasize the cost of power. Note that for low voltage tariffs (B2A and B2B), the minimum billed power of 15kW has been neglected.

With regards to the feed-in retribution of the PV production, 3 different rates have been selected based on what is currently applied in 2019 by energy providers. Figure 47 presents the feed-in tariff ranking of the 30 biggest DSOs in Switzerland [1].

[3] https://viteos.ch/wp-content/uploads/E_2019.pdf

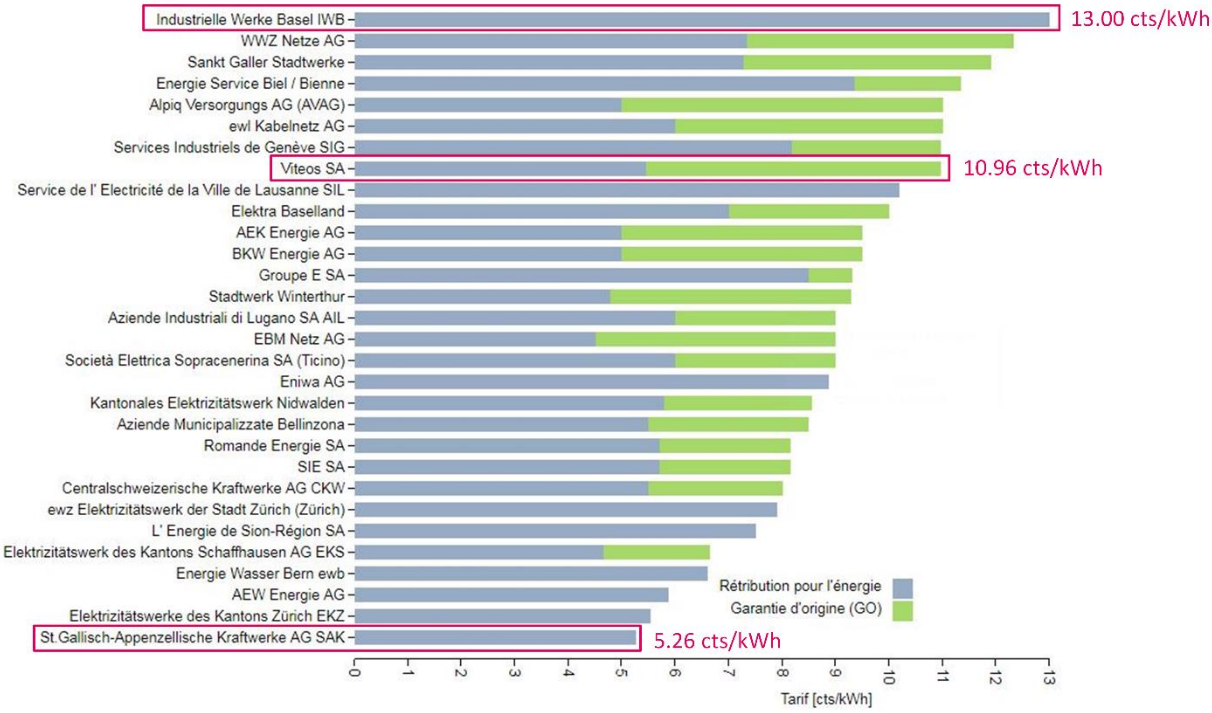

Figure 47: Ranking of feed-in retribution tariff of PV energy apply by Swiss DSOs in 2019 provided by VESE[4], with the selected tariff highlighted in red

The 3 selected rates for the assessment are highlighted in red. Thus, feed-in retributions of 13.00, 10.96 and 5.26cts/kWh will be compared in the assessment, without distinction between domestic, office and industrial buildings.

System

Three types of system will be compared:

- **DCSMART**: System with an optimally sized battery and using DCSMART control algorithm. The parameters of the control strategy are fixed and optimized over the year;
- **Buffer**: System with a battery of equivalent capacity but with a simple control strategy, the battery being used as an energy buffer. In case of over-production, the excess of energy is stored in the battery until it is full. In case of under-production, the lack of energy is down out of the battery until it is empty. This control scheme is what is used in most of the domestic battery system currently available on the market;
- **No battery**: System without battery

In order to get relevant results for the economic analysis, it is essential to account for the cost of the storage system and its lifespan. A convenient metrics to combine the two is the levelized cost of storage (LCOS). The LCOS [CHF/kWh] is defined as the total lifetime cost of an investment divided by the cumulated energy stored by this investment [20]. It thus represents the cost linked to the storage of one kWh of energy.

[4] https://www.vese.ch/fr/pvtarif/

According to [21], the LCOS for automotive batteries was evaluated at 0.15€/kWh (0.17CHF/kWh) in 2015 and expected to fall down to 0.05€/kWh (0.06CHF/kWh) in 2030. In this context, a slightly optimistic LCOS of 0.12CHF/kWh is used in the assessment. The impact of hardware design on LCOS – in particular any cost reductions arising from the direct interfacing in DC – are out of the scope of this evaluation because it is small compared to other factors we considered here: recent studies estimated the cost reduction from DC coupling between batteries and PV to be between 1.3% and 6% of the total system costs [22], [23].

Finally, the energy efficiency of the battery system is estimated to be constant, with a fixed round-trip efficiency of 90%.

Results

Optimal battery sizing

As announced earlier, the battery storage capacity of each building is optimized. This optimum is found by analysing the impact of the storage capacity (within reasonable bonds) on the yearly operating cost when using the DCSMART control strategy with optimum control parameters and a given set of tariffs. In the following, tariff of type B (i.e. B2B for domestic building and M1B for office and manufacturing building) and a feed-in tariff of 10.96CHF/kWh will be used for the assessment.

In Figure 48 is represented the yearly operating cost with respect to the battery capacity, for the DCSMART control in comparison to a system without storage. This exercise is performed for the three building types.

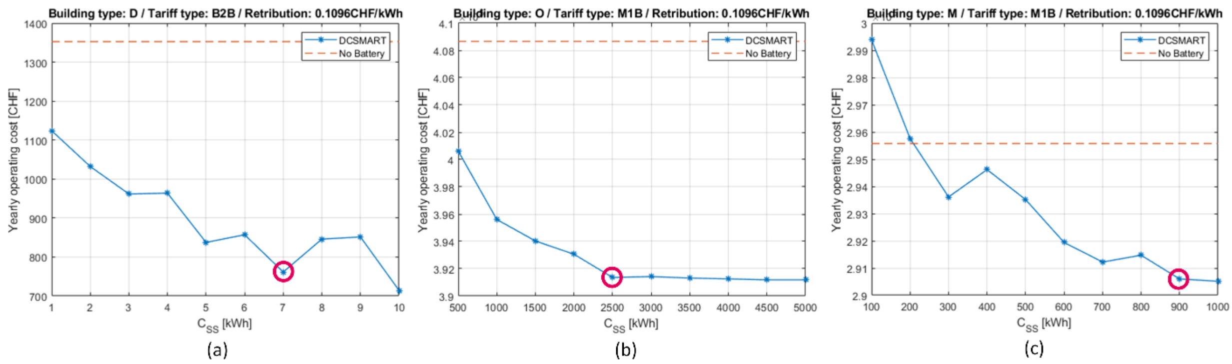

Figure 48: Yearly operating cost in function of storage capacity between D, for domestic building (a), office building (b) and manufacturing building (c).

Focusing on the domestic building results the optimum can be defined to 7kWh. Indeed, yearly cost reduction of 44% is already achieved with this storage capacity, while a savings increase of only 6% is achieved with a 10kWh battery.

Regarding the two other buildings, this optimum can be defined when the operating cost stabilized at 2.5MWh and 0.9MWh for respectively, the office building and the manufacturing building. It is interesting to observe that the optimum storage capacity for the commercial building is way higher than for the manufacturing one. Indeed, this effect is directly linked to the shape of the load profile and the capability the battery has to perform peak-shaving. The longer the peak-power, the higher the storage capacity need to shave the peak. Thus, since the manufacturing building has a higher load power consumption, with shorter peaks, a smaller storage capacity will be needed.

Effect of tariffs
The optimal storage capacity for each building being set, the effect of tariffs on the yearly operating cost can be assessed. In the analysis, a performance comparison is made between the DCMART system, a battery buffer system and a system without battery, and thus for each the 3 buildings.

Figure 49 presents, for each buildings, a yearly operating costs comparison in function of applied tariffs, and thus for every systems.

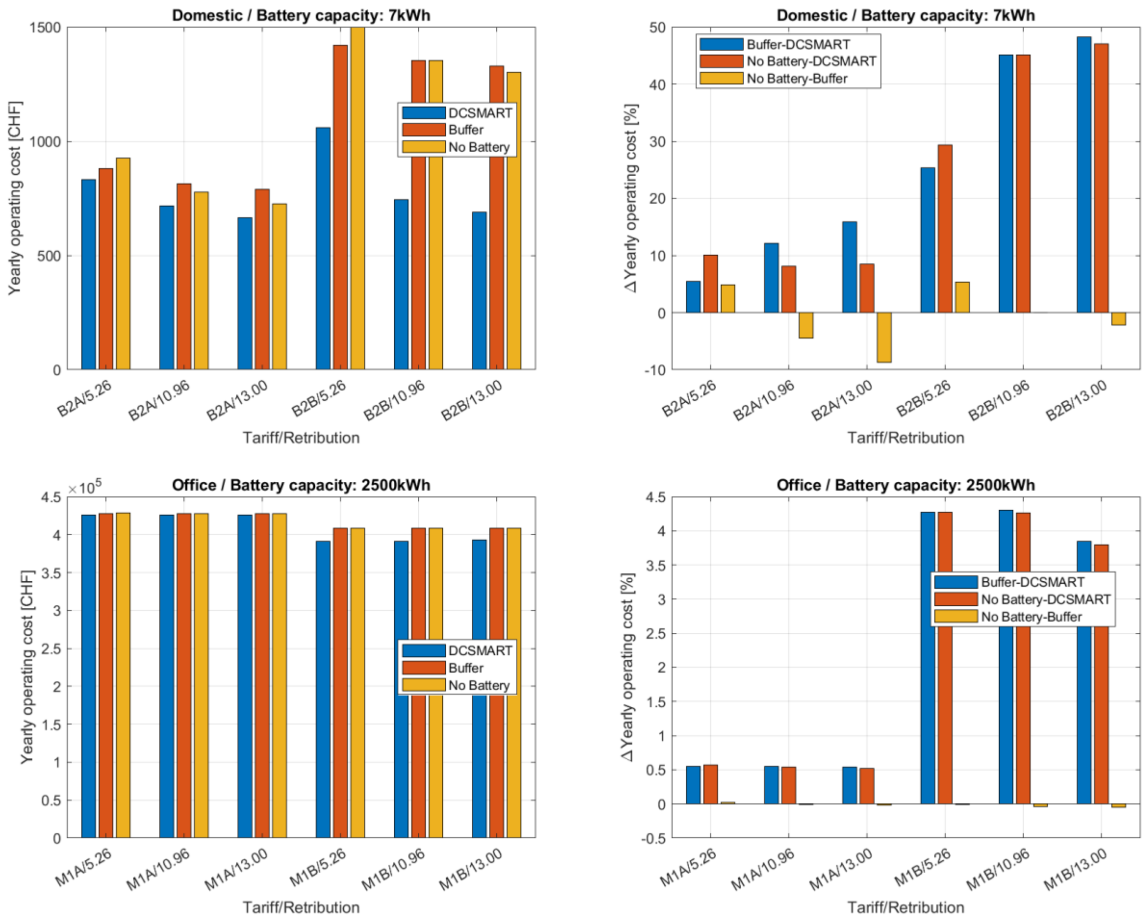

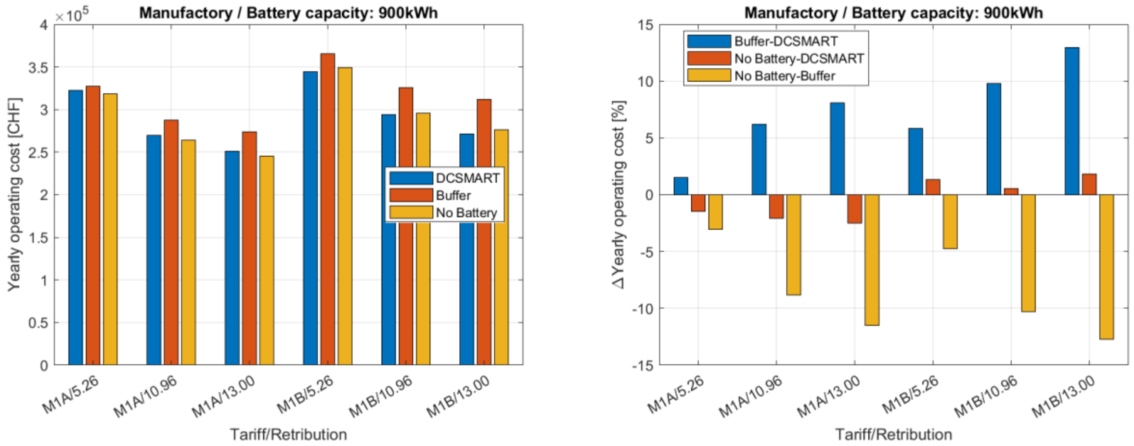

Figure 49: Yearly operating cost comparison between tariffs and systems for each buildings

Several comments can be made on these results:

- Compared to a simple buffer control, DCSMART is always, in those example, more economically profitable thanks to its ability to perform peak-shaving in addition to self-consumption.
- Buffer controlled battery are rarely profitable. This is the case only when feed-in tariff is low, when the benefit of doing self-consumption high. Indeed, as long as the difference between the energy purchase tariff and the feed-in tariff is lower than the LCOS of the battery, it is more profitable to “store in the grid” than in a battery.
- DCSMART strategy may be, in rare cases, worse than having no battery at all, especially when then power tariff is low compared to the energy tariff (i.e. manufacturing building type A tariffs)

In general, installing a DCSMART battery in a system without storage allows the following monetary savings for each building type:

- Domestic: 8.1% – 47.0%
- Office: 0.5% – 4.3%
- Manufacturing: -2.5% – 1.5%

Focusing on type B tariffs with a retribution of 10.96ct/kWh, an advanced assessment can be performed on the operating cost. Figure 50 depicts the split monthly operating cost for the office building (a) and the manufacturing building (b). The operating cost is divided between the cost of purchased energy, purchased power and the retribution for feed-in energy. The lower graph being the total monthly cost.

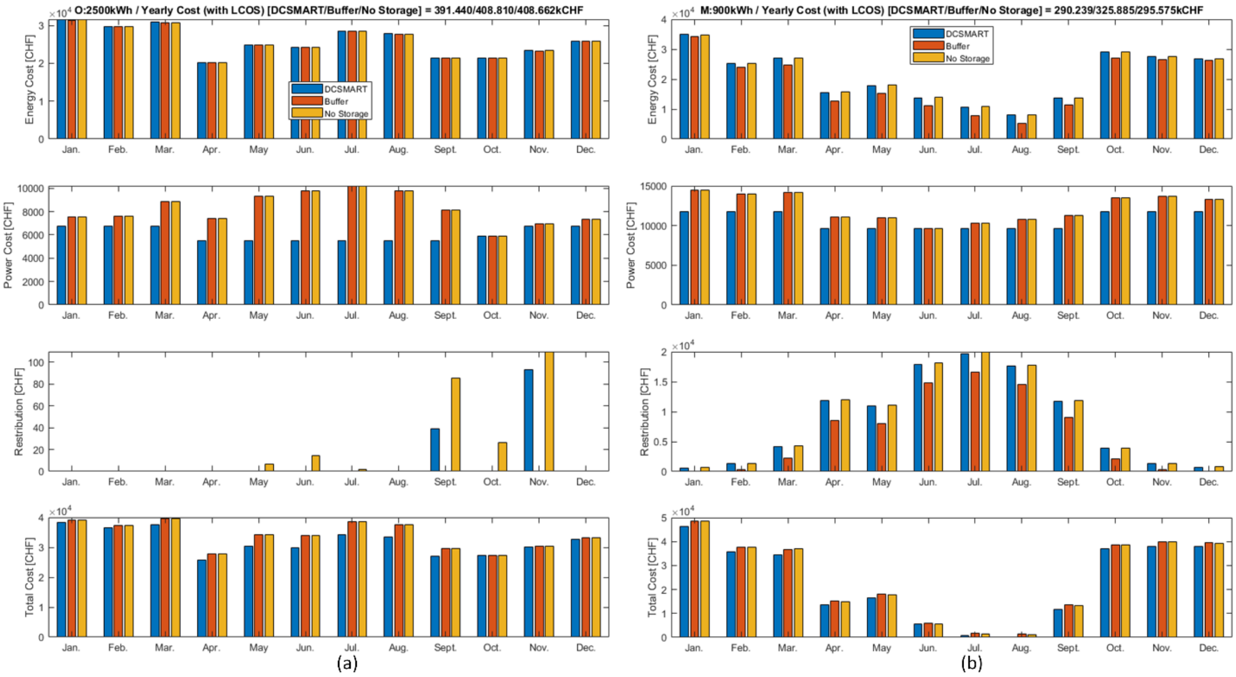

Figure 50: Split monthly operating cost for the office building (a) and the manufacturing building (b)

Once again, several conclusion can be drown from these results. On the one hand, and as expected, the buffer battery only reduce the energy cost and not the power cost. Since more energy is locally consumed, the retribution is automatically reduced. On the other hand, DCSMART reduces power cost and only slightly the energy cost. The balance between the decrease of one component or the other is optimized at the control strategy parameters selection. Since in those example the effort spent on the peak-shaving are generally more profitable, the storage capacity is almost always entirely dedicated to this service.

When focusing on the office building (Figure 50.a), it can be observed that no savings are performed in the energy cost with both battery systems. As the PV installation is small compared to the production, the self-consumption ratio (SCR) is already high (>99%) and cannot be significantly increased. Even though no saving can be made on the energy, significant savings are performed by DCSMART on the power cost. Finally, the almost non-existent retribution for PV energy feed-in validates the fact that a high majority of the energy produced locally is consumed locally.

Considering now the manufacturing building (Figure 50.b), with a higher share of PV production, the energy cost is decreased by the buffer battery. DCSMART, which optimally dedicates its storage capacity to peak-shaving, is slightly inefficient for energy cost reduction. The benefits of DCSMART are however visible on the power cost.

The same observations can be made on the detailed operating cost for the domestic building (Figure 51).

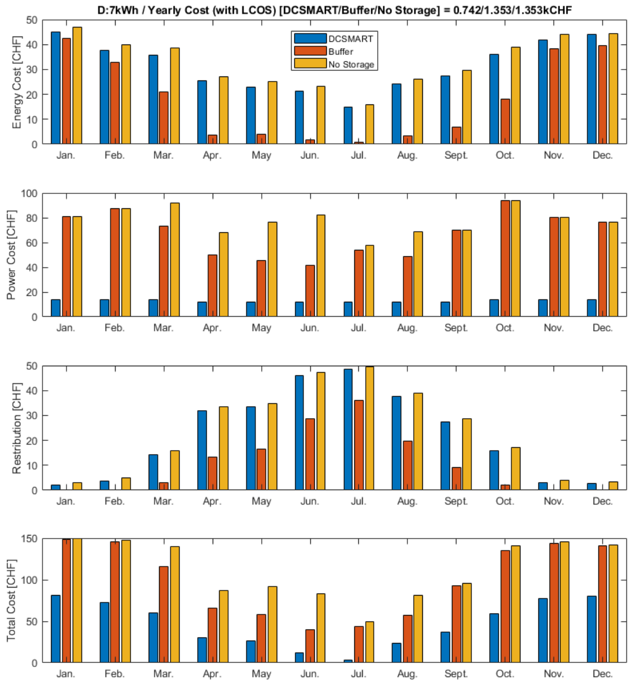

Figure 51: Split monthly operating cost for the domestic building

In this example, the effect is even more pronounced. The buffer battery highly decrease the energy cost while the DCSMART one highly decrease the power cost. However, since the share of the power cost on the overall operating cost is higher than the share of the energy cost, DCSMART solution is significantly more efficient in this situation than compared to the other buildings. Moreover, the ratio between the peaks and the average power consumption being substantially higher than for the other building, makes the peak-shaving easier to perform with a smaller battery.

This observation support the implementation of a DCSMART system for self-consumption communities. Indeed, such entities gather a small number of domestic consumers which aggregated consumption profile is still highly variable (high peak power). Since there energy consumption is higher, they generally have access to more tariffs than what a regular consumer has, tariffs that potentially include power billing.

Impact on grid power

On a technical point of view, the effect of the two battery control strategies on the grip power can be assessed. In Figure 52 is depicted the histogram of the grid power for each system and each building. They represent the duration in second during which a given power value has been exchange with the distribution grid, a positive value being a power extracted from the grid.

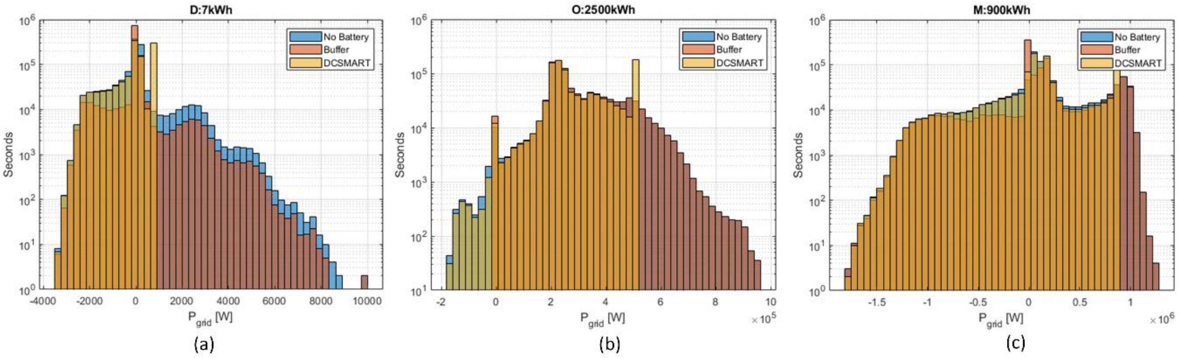

Figure 52: Histogram of the grid power for each system, for domestic (a), office (b) and manufacturing (c) building

These histograms allow to observe the peak-shaving performance of the DCSMART control strategy compared to the buffer one. Indeed, the yellow bars show that the power is limited at a given range, defined during the control parameters optimization process. This limitation is more important in the domestic building since the energy content of the high power is lower than for the other buildings. These figures also illustrate how inefficient is a buffer battery in performing peak-power.

Impact on the battery

From the battery point of view, its use is highly variable from one set-up to the next. Figure 53 illustrates the yearly evolution of the SoC for both buffer and DCSMART battery, thus for every building. Moreover, the number of equivalent cycle is depicted.

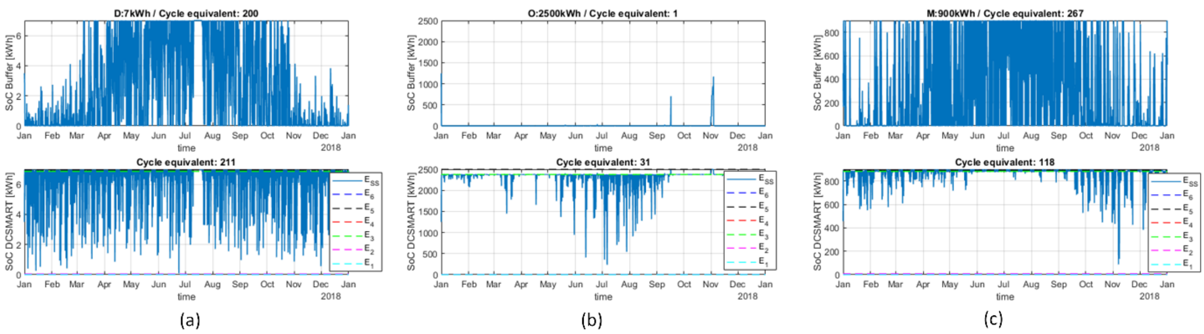

Figure 53: Yearly SoC profile for the buffer battery (upper graphs) and DCSMART battery (lower graph), for domestic (a), office (b) and manufacturing (c) building

Several comments can be made on these figures. Focusing first on the domestic building (a):

- The buffer battery is highly used since the PV production is significant compared to the load consumption and is mostly unmatched.
- The DCSMART battery is almost entirely used for peak-shaving in power extraction. Since the power profile of similar over the year (with comparable peaks), the yearly optimized control parameters are generally optimal every single day. This observation explains the good results obtained by DCSMART for the domestic building.
- The number of cycle is equivalent for both battery, but the average depth of discharge for DCSMART is lower. In addition to the better economic performance of the DCSMART, the control strategy will also slow the degradation of the battery.

Looking now at the office building (b):

- In perspective to its low PV production, the storage capacity is set absurdly big for the battery buffer. Indeed, the battery is never fully charged.
- The full storage capacity is only used few times (in summer) for DCSMART. Since the control parameters are only optimized once for the year, they are fixed based on the worst case and thus are highly conservative for the rest of the year. A more frequent update of the control parameters could then highly increase the performance of DCSMART.

Lastly, regarding the manufacturing building (c):

- The sizing of the buffer battery is more pertinent, with a high usage during the whole year due to the higher PV production.
- Same as before for the office building, the performance of DCSMART could be highly improved by updating the control parameters on a daily basis.
- It is however interesting to notice that with a reduction of 56% of the battery usage (in equivalent cycle), the DCSMART control achieves an economic performance 7% higher in average than the buffer battery.

Web service

In order to allow interested people to evaluate the economic benefit of the DCSMART solution, a web service is being developed. Although not finished yet, this development will continue beyond the completion date of the project.

This service will then allow the user to set consumption and production profiles, battery system specification and applied electricity tariffs. Based on this system configuration, an economic assessment will be performed. In more details, the user will have the possibility to:

- define a reference consumption profile from list of predefined typical profile and scale it to match a yearly energy consumption or the directly upload its own consumption profile;
- define a reference PV production profile based on its location and its PV installation specification or to directly upload its own production profile;
- set the specification of its storage system, including the storage capacity, its round-trip efficiency, its capacity in terms of cycling and its cost;
- select electricity tariffs among a predefined list or define them manually.

Once all these information are provided, the developed algorithm will simulate the system and provide a detailed presentation of the operating cost for:

- a system without battery;
- a system with a battery operated as energy buffer;
- a system with a battery of equivalent capacity operated with the DCSMART control strategy.

Perspectives, next steps

The DCSMART project paved the way for several projects and raised the interest of multiple industrials. Two projects are currently ongoing which purpose is to develop new iterations of this solution, aiming at a more compact, efficient, robust and safe system.

The first one is an EU Horizon 2020-funded project, called HYBUILD, which purpose is to develop innovative compact hybrid electrical/thermal storage systems for stand-alone and district connected buildings. CSEM's works focuses on the development of three electric demonstrators, linking through a DC bus, PVs, batteries, the distribution grid and a heat pump. They will be installed across Europe: in France, Spain and Cyprus. The developed devices will be compliant with the IEC 61439: Low-voltage switchgear and controlgear assemblies, necessary requirement in the perspective of a market launch.

The second one is the HiLo project. HiLo is a research & innovation unit for EMPA's NEST in the domains of ultra-lightweight construction and smart and adaptive building systems. This unit is planned as an office space, with HVAC, lighting, computers and fridge supplied in DC. As for the HYBUILD project, CSEM is working on the development of a DC microgrid to link the local PV installation, the distribution grid, a battery and the loads.

The perspectives in terms of industrial uptake are also promising. Four organisations have already expressed their interest in the DCSMART solution:

- A company active in automation technology, which manufactures PLCs and drives
- Neuchâtel's wastewater treatment plant included the option in its credit request for a major upgrade.
- An engineering contractor with interests in wider application for wastewater treatment plants.
- A distributor of battery system and renewable energy related products with interests in interfaces between automation and batteries.

Finally, a patent has been filled to protect the multi-service control strategy developed in the framework of the DCSMART project. The validation process is ongoing but the first feedbacks from the European patent office are promising.

Conclusions

The Swiss demonstration site of the DCSMART project has been operational since December 2018, providing several months of data. Its control strategies were initially validated in simulation. Several modifications proved necessary to adapt to the physical reality of the demonstration site, in particular to adapt to the limited resolution of the battery SoC provided by the battery management system, and the limited current capability of the battery storage system. Some imperfections remain, such as a non-negligible standby power consumption (84 W) and small power oscillations in specific cases. However, all the features designed in the system have been successfully validated, with the system behaving as expected in all cases.

The DCSMART solution implemented on the Swiss demonstration site is therefore capable of providing multiple services to the public distribution grid and to the end users (increase in self-consumption of locally-produced electricity, peak shaving, and reduction in power ramp rates). The economic gains calculated in D6.1 and in this document are therefore full achievable with this solution.

References

[1] F. Colville, “The PV Industry in 2013: Top-10 Questions/Trends,” presented at the PV Production and Battery Forum 2013, Paris, 02-Oct-2013.

[2] M. Rekinger, F. Thies, G. Masson, and S. Orlandi, “Global market outlook for solar power 2015-2019,” SolarPower Europe, Brussels, Jun. 2015.

[3] R. Komsi, “Energy storage grid connection with power electronics,” presented at the EERA Smart Grid R&D Workshop, Milan, Italy, 28-Jun-2012.

[4] M. Salato and U. Ghisla, “Optimal power electronic architectures for DC distribution in datacenters,” presented at the 1st IEEE international conference on DC microgrids, Atlanta, GA, USA, Jun-2015.

[5] M. Johnson, “ECO priority source: DC micro-grids in telecom sites,” presented at the 1st IEEE international conference on DC microgrids, Atlanta, GA, USA, Jun-2015.

[6] EMerge Alliance, “380Vdc Architectures for the Modern Data Center,” EMerge Alliance, San Ramon, CA, USA, 2013.

[7] ETSI Technical Committee Environmental Engineering, “Power supply interface at the input to telecommunications and datacom (ICT) equipment; Part 3: Operated by rectified current source, alternating current source or direct current source up to 400 V; Sub-part 1: Direct current source up to 400 V,” ETSI, Sophia Antipolis, European Standard EN 300 132-3-1-V2.1.1, Feb. 2012.

[8] U. Boeke and M. Wendt, “DC power grids for buildings,” presented at the 1st IEEE international conference on DC microgrids, Atlanta, GA, USA, 09-Jun-2015.

[9] Fraunhofer IISB, “DC Micro Grid Control System for optimized usage of renewable energy in buildings,” Fraunhofer Institute for Integrated Systems and Device Technology IISB, Erlangen, Germany, Brochure, 2014.

[10] A. Lana, A. Pinomaa, P. Nuutinen, T. Kaipia, and J. Partanen, “Control and monitoring solution for the LVDC power distribution network research site,” presented at the 1st IEEE international conference on DC microgrids, Atlanta, GA, USA, Jun-2015.

[11] E. Rodriguez-Diaz, X. Su, M. Savaghebi, J. C. Vasquez, M. Han, and J. M. Guerrero, “Intelligent DC microgrid living laboratories: A Chinese-Danish collaboration project,” presented at the 1st IEEE international conference on DC microgrids, Atlanta, GA, USA, Jun-2015.

[12] “Solving problems with the large-scale introduction of solar power by using HEMS,” *Japan Smart City*, 15-Feb-2013. [Online]. Available: http://jscp.nepc.or.jp/article/jscpen/20130214/340272/index.shtml. [Accessed: 27-Feb-2013].

[13] D. Fregosi *et al.*, “A comparative study of DC and AC microgrids in commercial buildings across different climates and operating profiles,” in *2015 IEEE First International Conference on DC Microgrids (ICDCM)*, 2015, pp. 159–164.

[14] M. R. Starke, L. M. Tolbert, and B. Ozpineci, “AC vs. DC distribution: A loss comparison,” presented at the IEEE/PES Transmission and Distribution Conference and Exposition, Chicago, IL, 2008, pp. 1–7.

[15] Z. Liu and M. Li, “Research on Energy Efficiency of DC Distribution System,” *AASRI Procedia*, vol. 7, pp. 68–74, 2014.

[16] V. Musolino, P.-J. Alet, L. Piegari, L.-E. Perret-Aebi, and C. Ballif, “Alleviating power quality issues when integrating PV into built areas: design and control of DC microgrids,” in *IEEE first international conference on DC microgrids*, Atlanta, GA, USA, 2015, pp. 102–107.

[17] J. von Appen, M. Braun, T. Stetz, K. Diwold, and D. Geibel, “Time in the Sun: The Challenge of High PV Penetration in the German Electric Grid,” *IEEE Power Energy Mag.*, vol. 11, no. 2, pp. 55–64, Mar. 2013.

[18] A. V. den Bossche, B. Meersman, and L. Vandevelde, “Fundamental tarification of electricity,” in *2009 13th European Conference on Power Electronics and Applications*, 2009, pp. 1–7.

[19] “EnerNOC Open :: Data.” [Online]. Available: https://open-enernoc-data.s3.amazonaws.com/anon/index.html. [Accessed: 03-May-2019].

[20] I. Pawel, “The Cost of Storage – How to Calculate the Levelized Cost of Stored Energy (LCOE) and Applications to Renewable Energy Generation,” *Energy Procedia*, vol. 46, pp. 68–77, Jan. 2014.
[21] W. Hoffmann, “Importance and Evidence for Cost Effective Electricity Storage,” presented at the 29th European Photovoltaic Solar Energy Conference and Exhibition, Amsterdam, The Netherlands, 2014.
[22] K. Ardani, E. O’Shaughnessy, R. Fu, C. McClurg, J. Huneycutt, and R. Margolis, “Installed Cost Benchmarks and Deployment Barriers for Residential Solar Photovoltaics with Energy Storage: Q1 2016,” National Renewable Energy Laboratory, Golden, Colorado, USA, Technical Report NREL/TP-7A40-67474, Feb. 2017.
[23] R. Fu, T. Remo, and R. Margolis, “2018 U.S. Utility-Scale Photovoltaics-Plus-Energy Storage System Costs Benchmark,” *Renew. Energy*, p. 32, 2018.

Annexe

– Annexe 1: D6.1 (ERA-Net deliverable)
– Annexe 2: D6.2 (ERA-Net deliverable)

List of abbreviations

Abreviation	Français	English
BMS	Système de gestion de batterie	Battery management system
DC	Courant continu	Direct current
DSO	Gestionnaire de réseau de distribution	Distribution system operator
ESS	Système de stockage d’énergie	Energy storage system
GHI	Irradiance horizontale globale	Global horizontal irradiance
HVAC	Chauffage, ventilation et climatisation	Heating, ventilation and air-conditioning
LCOS	Coût de stockage nivelé	Levelized cost of storage
LPG	Générateur de profile de charge	Load profile generator
PV	Photovoltaïque	Photovoltaic
SCR	Taux d’auto-consommation	Self-consumption ratio
SoC	Etat de charge	State of charge
WTP	Station d’épuration	Water treatment plant